Molecular Therapy
Nucleic Acids
Original Article

Astrocyte-targeted siRNA delivery by adenosine-functionalized LNP in mouse TBI model

Hai Xiao,[1] Odmaa Amarsaikhan,[1] Yunwang Zhao,[1] Xiang Yu,[1] Xin Hu,[1] Shuqin Han,[1] Chaolumen,[1] and Huricha Baigude[1]

[1]Inner Mongolia Key Laboratory of Mongolian Medicinal Chemistry, School of Chemistry & Chemical Engineering, Inner Mongolia University, Hohhot, Inner Mongolia 010020, P.R. China

Traumatic brain injury (TBI) induces pro-inflammatory polarization of astrocytes and causes secondary disruption of the blood-brain barrier (BBB) and brain damage. Herein, we report a successful astrocyte-targeted delivery of small interfering RNA (siRNA) by ligand functionalized lipid nanoparticles (LNPs) formulated from adenosine-conjugated lipids and a novel ionizable lipid (denoted by Ad4 LNPs). Systemic administration of Ad4 LNPs carrying siRNA against TLR4 to the mice TBI model resulted in the specific internalization of the LNPs by astrocytes in the vicinity of damaged brain tissue. A substantial knockdown of TLR4 at both mRNA and protein levels in the brain was observed, which led to a significant decrease of key pro-inflammatory cytokines and an increase of key anti-inflammatory cytokines in serum. Dye leakage measurement suggested that the Ad4-LNP-mediated knockdown of TLR4 attenuated the TBI-induced BBB disruption. Together, our data suggest that Ad4 LNP is a promising vehicle for astrocyte-specific delivery of nucleic acid therapeutics.

INTRODUCTION

Traumatic brain injury (TBI) is caused by traumatic events such as falls and traffic accidents, leading to the death of neural cells at the impact site.[1] TBI often induces serious effects on neurological function and is one of the leading causes of disability and mortality.[2,3] Astrocytes are the most abundant glial cells in the brain that greatly contribute to tissue repair after TBI.[4] Astrocytes are activated in response to TBI, leading to inflammation of nerve tissue, which often causes secondary brain damage.[5] In brain lesions, activated astrocytes polarized into pro-inflammatory or anti-inflammatory phenotypes during neuroinflammation.[6–8] The pro-inflammatory phenotype promotes inflammatory response, oxidative stress, induces immune response, and extends damage range.[9,10] The anti-inflammatory phenotypic glial cells release anti-inflammatory cytokines that have neuroprotection effects.[11–13] Glial cell polarization can be regulated by therapeutics. For example, Maraviroc, a CCR5 antagonist, can alleviate neurological deficits and restore function after TBI injury by regulating the polarization of microglia.[14,15]

However, treatments for TBI encounter a variety of obstacles, including reaching target tissue and the blood-brain barrier (BBB).[16] TBI-induced brain damage results in the release of cell debris and intact or partially degraded biomolecules that act as the endogenous ligands for the pattern recognition receptors (PRRs). For example, sulfatides, the natural membrane glycolipids in mammals, directly activate Toll-like receptor 4 (TLR4) and its coreceptor myeloid differentiation factor-2 (MD2), trigger MyD88-dependant signaling, and upregulate the expression of tumor necrosis factor alpha (TNFα) in macrophages.[17] Previously, we created a mannose receptor (MR)-specific lipid nanoparticle (LNP) by conjugating mannose to DoGo lipid[18] and demonstrated that MR-mediated endocytosis of LNP carrying small interfering RNA (siRNA) against TLR4 can efficiently reprogram the polarization of oxygen-glucose deprived (OGD) microglia *in vitro*.[19]

RNA interference (RNAi) is a highly efficient tool that selectively manipulates gene expression, and therefore provides a potential therapeutic approach to a broad spectrum of diseases.[20–22] The large molecular weight and negative charge of siRNA requires delivery systems to overcome these barriers.[23–25] LNPs are the most advanced delivery system for RNA therapeutics, including siRNA drugs[21,26] and mRNA vaccines.[27,28] LNP delivery systems consisting of ionizable lipids are positively charged at acidic pH and neutral at physiological pH, making them more likely to encapsulate siRNA and escape endosomes,[29] and reduced immunogenicity or toxic effects.[30] The tissue targeting efficiency of the passive LNP delivery systems or naked RNA molecules could be improved by decoration of active targeting moieties,[31–34] such as monoclonal antibodies,[35,36] peptides,[37–39] aptamers,[40] or receptor ligands.[41–43] Among them, receptor ligands have the advantages of low cost, small size, low immunogenicity, high stability, and relatively easier chemical modification.[32] And, the binding affinity of the receptor ligand to the target is generally low, resulting in weak and reversible ligand/target interactions, but this weak binding ability may favor endocytosis and tissue penetration. If the binding is too strong, the ligand nanocarriers may become trapped in the tissue or transported to the

Received 8 August 2023; accepted 18 October 2023;
https://doi.org/10.1016/j.omtn.2023.102065.

Correspondence: Huricha Baigude, School of Chemistry & Chemical Engineering, Inner Mongolia University, Hohhot 010020, P.R. China.
E-mail: hbaigude@imu.edu.cn

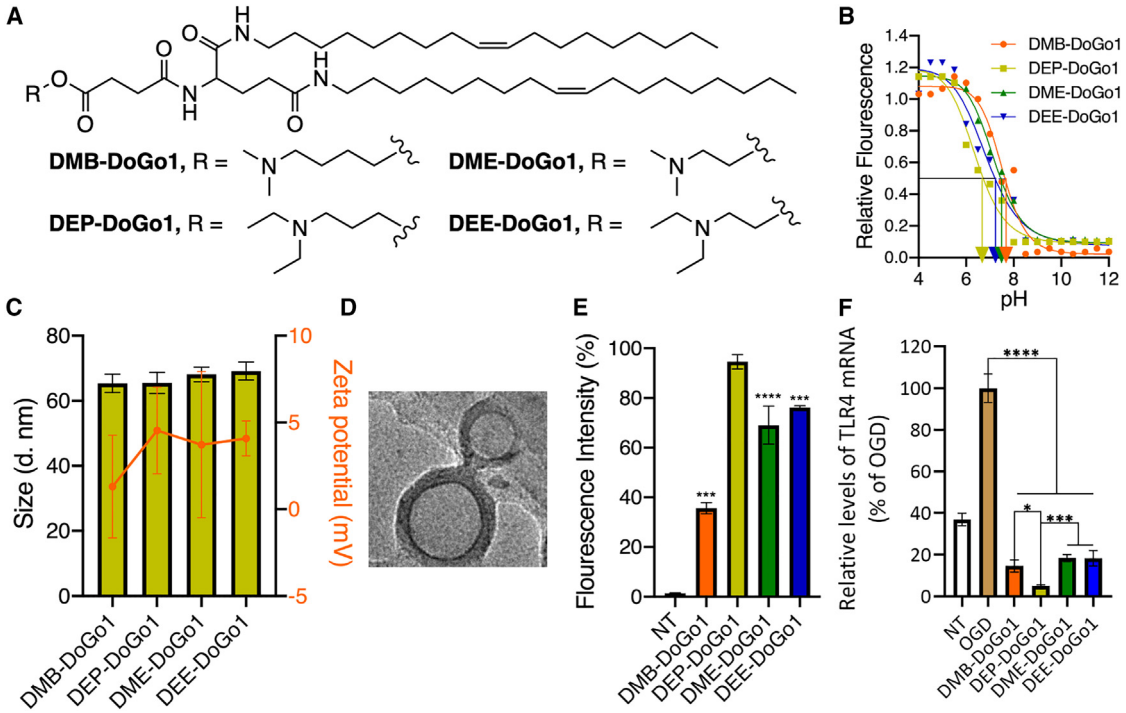

Figure 1. Characterization and screening for *in vitro* siRNA delivery of the DoGo-derived ionizable lipids

(A) Structures of DoGo-derived ionizable lipids. (B) pKa value of the DoGo-derived ionizable lipids. (C) The particle size and zeta potential of LNP formulated from DoGo-derived ionizable lipids. (D) TEM images of the LNP formulated from DoGo-derived ionizable lipids. (E) Cellular uptake efficiency of LNP formulated from DoGo-derived ionizable lipids. (F) siRNA transfection efficiency of LNP formulated from DoGo-derived ionizable lipids. OGD-treated C8-D1A cells were treated with the LNPs carrying siRNA against TLR4, respectively. Twenty-four hours later, the mRNA level of TLR4 in the cells was measured by RT-qPCR. *p < 0.05; **p < 0.01; ***p < 0.001; ****p < 0.0001.

lysosome for degradation, which is a challenge for antibody-modified delivery systems.[41,44] Adenosine receptors (ARs), also known as P1 receptors, are a class of purine G protein-coupled receptors with adenosine as endogenous ligand,[45] and highly expressed in the brain.[46]

In this study, we designed an active targeting LNP system by formulating novel DoGo-derived ionizable lipids and adenosine-conjugated DoGo lipids. DoGo lipids are a series of cationic peptidomimetics-conjugated lipids that have great siRNA delivery efficiency.[18] We previously demonstrated that DoGo-derived LNP can specifically deliver siRNA to microglia in a mouse model of middle cerebral artery occlusion and induce efficient knockdown of TLR4.[47] We hypothesize that adenosine functionalized LNP would be internalized by astrocytes via ARs, which are highly expressed on astrocytes cell surface. We discovered that astrocyte-targeted Ad LNPs can deliver siRNA against TLR4, reprogram astrocyte polarization, and attenuate TBI-induced secondary brain injury and enhance the integrity of the BBB in a mice TBI model.

RESULTS

Our previous studies revealed that LNP or polymeric NP can infiltrate brain tissue via transiently permeable BBB in a mice stroke model and deliver siRNA to specific glial cell populations to regulate their polarization.[47,48] The goal of the present study was to create an astrocyte targeting LNP carrier for siRNA that can modulate the polarization of the glial cells after brain damage. Astrocytes are a major population of glial cells in the CNS, and they express all four subtypes of adenosine receptor. Astrocytes are a main source of adenosine during episodes of ischemia, injury, and inflammation.[49,50] Our previous study demonstrated that AR can be utilized for the receptor-mediated siRNA delivery.[51]

Ionizable lipids with different chemical properties have been studied since 2008. Ionizable lipids can be divided into unsaturated ionizable lipids, multi-tail ionizable lipids, ionizable polymer-lipids, biodegradable ionizable lipids, and branched-tail ionizable lipids.[52] So far, the Food and Drug Administration-approved lipids used to deliver siRNA and mRNA all belong to ionizable lipids, for example, DLin-MC3-DMA or MC3 which are tertiary amine structures with two unsaturated tails.[53] DoGo lipids are peptidomimetics conjugated with lipids that have appreciable nucleic acids delivery efficiency and negligible cytotoxicity.[18] To further enhance the *in vivo* siRNA delivery efficiency of DoGo lipids, we synthesized four ionizable DoGo derivative lipids (denoted by DMB-DoGo1, DEP-DoGo1, DME-DoGo1, and DEE-DoGo1). After the structure of the ionizable lipids was confirmed by NMR spectroscopy (Figure 1A, supporting information materials and methods), we measured the pKa value of each individual lipid (Figure 1B). Surface pKa value is one of the critical parameters for LNP in terms of siRNA delivery ability,[54,55] because gene silencing efficiency was strongly correlated with pKa, with the optimal pKa values

Table 1. Characterization of physicochemical properties of LNP prepared from DoGo-derived ionizable lipids

LNP	Size (nm)[a]	PDI	Zeta potential (mV)	Encapsulation efficiency (%)	pKa of ionizable lipid[b]
DMB-DoGo1	65.4 ± 2.85	0.23 ± 0.04	1.92 ± 2.21	88.6 ± 0.50	7.67
DEP-DoGo1	65.5 ± 3.21	0.21 ± 0.03	4.50 ± 2.56	97.8 ± 0.08	6.72
DME-DoGo1	68.1 ± 2.21	0.24 ± 0.07	3.72 ± 4.22	94.3 ± 0.71	7.45
DEE-DoGo1	69.2 ± 2.76	0.30 ± 0.06	4.00 ± 1.35	97.5 ± 0.30	7.19

[a]Measured by Dynamic Light Scattering.
[b]Determined by TNS assay.

being around 7.0.[55] For example, SM-102 lipid used in Moderna mRNA COVID-19 vaccine has a pKa value of 6.68, and pKa value of DLin-MC3-DMA was 6.44. DoGo-derived ionizable lipids showed pKa value ranging from 6.72 to 7.67 (Table 1). Finally, we observed the stability of DEP-DoGo1 lipid in full medium. The mixtures of full medium and lipids at 6/1 (v/v), were observed after 0, 1, 2, and 3 days, respectively, and the results showed that DEP-DoGo1 lipid had high stability in full medium (Figure S1).

Next, we prepared LNP derived from each of the DoGo-derived lipids by mixing with DSPC, cholesterol, DMG-PEG_{2000}, and siRNA, respectively, using an extrusion method. DEP-DoGo1 LNP showed the highest encapsulation efficiency (Tables 1 and S1). All LNPs showed a favorable particle size ranging from 65 to 69 nm and low zeta potential ranging from 1.92 to 4.50 mV (Figures 1C, 1D, and S2; Table 1). The particle size distribution and morphology of LNPs are among the crucial factors that determine the circulation time, biodistribution, stability, and clearance of LNPs.[56] LNPs with a diameter of 45 nm were most effective for subcutaneous administration, while a diameter of 80 nm makes the LNPs most effective for intravenous administration.[57] LNPs with a particle size of less than 100 nm can pass through capillary pores and reach the blood circulation, which is a key step in crossing the vascular barrier immunogenicity.[58]

To evaluate the *in vitro* siRNA delivery efficiency of the DoGo-derived lipids, we first treated C8-D1A cells with the DoGo-derived LNP carrying FAM-labeled siRNA, respectively, and quantified the cellular uptake efficiency of each LNP by flow cytometry. C8-D1A cells are an astrocyte cell line isolated from mouse cerebellum that express a high level of ARs. The OGD is an *in vitro* model for stroke that induces neuronal injury. DEP-DoGo1-based LNP showed the highest cellular uptake by the C8-D1A cells (Figures 1E and S3). On the OGD-treated C8-D1A cells, DEP-DoGo1-based LNP carrying siRNA against TLR4 induced 89% decrease in TLR4 mRNA level, the highest among the four LNPs (Figure 1F). These results demonstrated that DEP-DoGo1 has the most favorable physicochemical properties and *in vitro* transfection efficiency, therefore it can be used as the first choice of ionizable lipid for subsequent formulation of receptor targeting LNPs.

To achieve AR receptor-mediated siRNA delivery to astrocytes, we first synthesized adenosine functionalized lipids by conjugating either single adenosine moiety (denoted by Ad1-DoGo1) or four adenosine moieties (denoted by Ad4-DoGo4) to the DoGo1 and DoGo4, respectively (supporting information materials and methods, Figures 2A and 2B). Next, we incorporated Ad-DoGo lipids into the DEP-DoGo1-based LNP as an auxiliary lipid to prepare the AR-targeting LNP and obtained eight formulations based on variant ratio of DSPC and Ad-DoGo lipids (Table 2, denoted by Ad1-1 to Ad1–4 LNP or Ad4-1 to Ad4-4 LNP). The subsequent characterizations of Ad4-3 LNP revealed that incorporation of Ad-DoGo lipids increased the pKa of the resulting LNP to 7.51 and 7.05, respectively (Figure 2C). Although the encapsulation efficiency of DEP-DoGo1 LNP with or without adenosine-conjugated lipids did not change, the particle size increased and zeta potential decreased (Figure 2D and Table S2). However, transmission electron microscopy (TEM) observation of the morphology indicated that Ad4 LNP was more homogeneous compared with the Ad1 LNP (Figure 2E).

The screening of the transfection efficiency of the Ad LNPs on C8-D1A cell lines revealed that increasing the adenosine moiety in the LNP can enhance the transfection efficiency, and Ad4 LNPs had significantly higher transfection efficiency compared with Ad1 LNPs. For example, Ad4-3 LNP and Ad4-4 LNP, which contain a higher ratio of Ad4-DoGo4 lipid, showed higher transfection rate and exhibited superior siRNA delivery efficiency compared with all Ad LNPs (Figures 3A, S4, and S5). The cellular uptake of Ad4-3 LNP and Ad4-4 LNP measured by flow cytometry showed no significant difference between the two LNPs. To fine-tune Ad4 LNPs for the optimal transfection efficiency, we next compared the *in vitro* siRNA delivery efficiency of Ad4-3 and Ad4-4 LNPs. To do this, we transfected OGD-treated C8-D1A cells with the Ad4-3 and Ad4-4 LNPs carrying siRNA against TLR4, respectively, using a series of siRNA concentration (10, 5, 1, and 0.5 nM). RT-qPCR and western blot analysis revealed that Ad4-3-mediated siRNA delivery to the astrocyte cell line had the best gene silencing efficiency at both the mRNA and protein level of the target gene (Figures 3B, 3C, and S6).

Next, we evaluated the astrocyte AR specificity of Ad4-3 LNP. To do this, we first conducted a competitive blocking experiment. We selected AMP, the natural ligand for ARs, as the receptor binding competitor to evaluate the AR receptor binding specificity of Ad4-3 LNP using GMP as negative controls. C8-D1A cells were pretreated with either AMP or GMP, and then treated with Ad4-3 LNP carrying FAM-labeled siTLR4. Four hours later, the transfection efficiencies were quantitatively analyzed by flow cytometry. The results showed that cellular uptake of Ad4-3 LNP was significantly inhibited by AMP but not by GMP

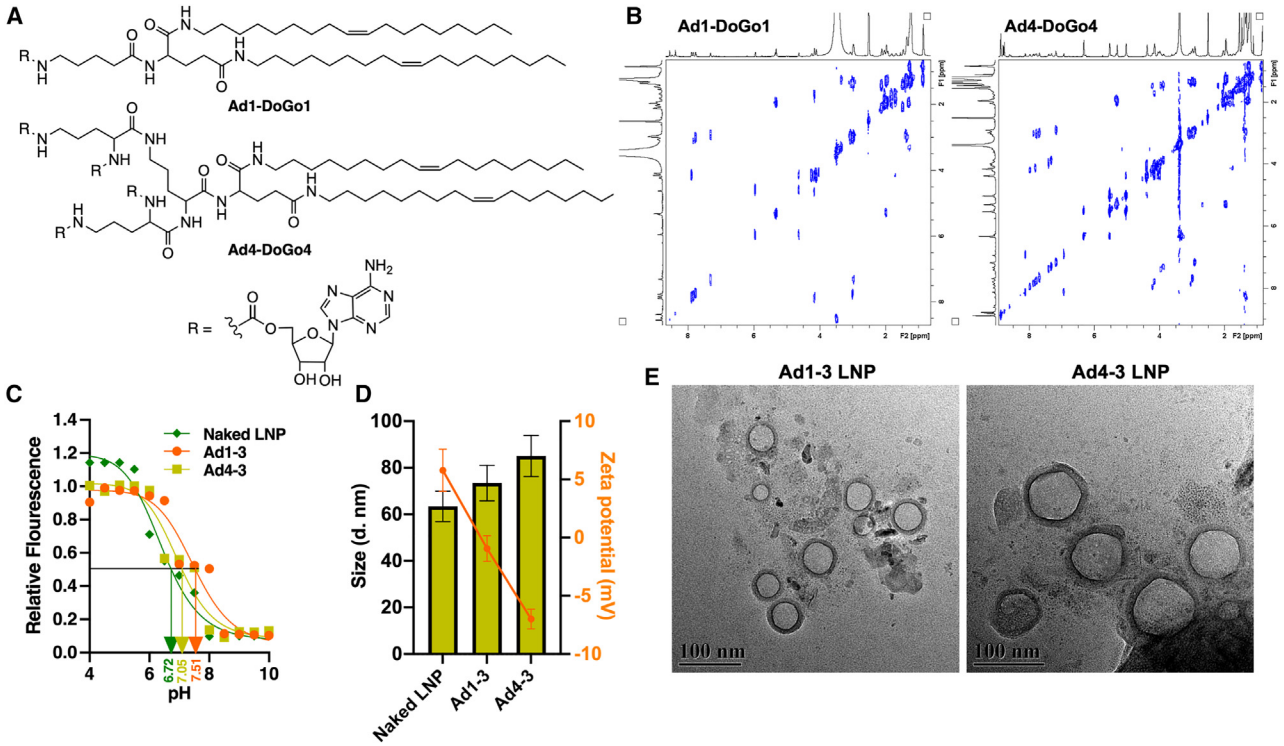

Figure 2. Screening and *in vitro* siRNA delivery of the adenosine functionalized LNPs

(A) Structures of Ad1-DoGo1 and Ad4-DoGo4. (B) Measurement of pKa value of the naked LNP, Ad1–3 LNP, and Ad4-3 LNP. (C) Measurement of pKa value of the Ad LNPs. (D) The particle size and zeta potential of naked LNP, Ad1–3 LNP, and Ad4-3 LNP. (E) TEM images of the Ad1-3 LNP and Ad4-3 LNP.

(Figure 3D), suggesting that Ad4-3 LNP may have been internalized through AR receptor-mediated endocytosis. To further confirm the AR specificity of Ad4-3 LNP, we knocked down each individual AR (i.e., A_1R, $A_{2A}R$, $A_{2B}R$, and A_3R) using antisense oligonucleotide (ASO) to silence the corresponding target gene in C8-D1A cells, respectively. A mixture of four ASOs was also used to knock down all four ARs simultaneously. Upon confirmation of AR knockdown 24 h after the transfection of ASO (Figure S7), we treated the cells with Ad4-3 LNP carrying FAM-labeled siTLR4. Four hours later, the cellular uptake of Ad4-3 LNP in each treatment group was quantified by flow cytometry. The results showed that knockdown of each individual AR decreased the uptake of Ad4-3 LNP by 55%–65% (Figure 3E). Significantly, a combined knockdown of all ARs simultaneously in the cells resulted in 90% decrease in the internalization of Ad4-3 LNP, confirming the AR receptor-dependent uptake of Ad4-3 LNP by C8-D1A cells.

Furthermore, we performed a temperature-dependent internalization assay to investigate the energy dependency of Ad4-3 LNP uptake by C8-D1A cells. To do this, we treated C8-D1A cells with Ad4-3 LNP carrying FAM-labeled siRNA at either low temperature (4°C) or normal incubation temperature (37°C), followed by the measurement of fluorescence intensity of the cells by flow cytometry. The results showed that the fluorescence intensity at 4°C was lower than at 37°C at all measured time points, and the overall cellular uptake increased with time, indicating that the energy-dependent uptake occurred at 37°C (Figure 3F). This result can be explained as follows: the increase of fluorescence intensity at 4°C reflected the number of Ad4-3 LNPs binding to ARs on the cell surface, and at 37°C reflected the endocytic uptake of Ad4-3 LNP plus the amount of binding to the cellular surface, suggesting that Ad4-3 LNP was internalized by the C8-D1A cells through an energy-dependent endocytic process.

Finally, we performed immunocytochemistry (ICC) to further confirm AR-mediated internalization of Ad4-3 LNP by astrocyte cell line. Because $A_{2A}R$ is the most abundantly expressed AR in C8-D1A cells, we used it as a representative receptor for ICC analysis. We first treated C8-D1A cells with Ad4-3 LNP carrying FAM-labeled siRNA. Four hours later, we stained the cells with anti-$A_{2A}R$ antibody and Alexa Flour 594 dye-conjugated secondary antibody. After staining the nuclei with DAPI, we observed the cells under confocal microscope. Clear overlaying of $A_{2A}R$ (red) and Ad4-3 LNP (green) was observed, demonstrating that Ad4-3 LNPs bound to $A_{2A}R$ and were subsequently internalized by C8-D1A cells via $A_{2A}R$-mediated internalization (Figure 3G). These results confirmed that Ad4-3 LNPs were internalized by the astrocyte cell line via AR-mediated endocytosis.

To investigate the brain-targeting ability and astrocyte specificity of Ad4-3 LNP *in vivo*, we systematically administrated Ad4-3 LNP carrying FAM-labeled siTLR4, or naked FAM-labeled siTLR4 to the mouse TBI model, and PBS to the healthy mouse as a negative control.

Table 2. Formulation of Ad1 LNPs and Ad4 LNPs

Formulation	Variable (molar %)		Constant (molar %)		
	Adenosine lipid (molar %)	DSPC	DEP-DoGo1	Cholesterol	DMG-PEG$_{2000}$
Naked LNP	0	10			
Ad1-1	Ad1-DoGo1 (2.5)	7.5			
Ad1-2	Ad1-DoGo1 (5.0)	5			
Ad1-3	Ad1-DoGo1 (7.5)	2.5			
Ad1-4	Ad1-DoGo1 (10)	0	50	38.5	1.5
Ad4-1	Ad4-DoGo4 (2.5)	7.5			
Ad4-2	Ad4-DoGo4 (5.0)	5			
Ad4-3	Ad4-DoGo4 (7.5)	2.5			
Ad4-4	Ad4-DoGo4 (10)	0			

Twenty-four hours after intravenous (i.v.) injection, we collected major organs (liver, lung, spleen, kidney, and brain) and observed the fluorescence intensity by UVP Ibox Scientia. The strongest fluorescence signal was detected in brain of an Ad4-3 LNP-treated mouse. When we quantified by ImageJ, we found that the brain harvested from the Ad4-3 LNP treatment mouse had significantly stronger fluorescence intensity than naked siRNA and PBS-treated mouse (Figures 4A and S8), suggesting that Ad4-3 LNP enters the brain via disrupted BBB. To further investigate the neural cell specificity of Ad4-3 LNP, we observed the fluorescence signal of peri-infarct region of brain tissue slides. The strongest green signal of FAM was detected in peri-infarct region, mostly colocalized with GFAP-positive cells (Figures 4B and 4C), indicating that Ad4-3 LNP specifically delivered siRNA to astrocytes in the peri-infarct region in the ipsilateral cortex. No colocalized fluorescence signal of Iba1 and NeuN (Figure S9) was observed, suggesting that the Ad4-3 LNP penetrated the BBB in the TBI model of mice and actively entered the astrocyte through AR-mediated endocytosis.

Next, we measured the astrocyte-specific gene silencing efficiency of Ad4-3 LNP-mediated siRNA delivery at mRNA and protein levels. RT-qPCR and western blot analysis revealed significant knockdown of TLR4 at both mRNA and protein levels in the lesion region (Figures 4D and 4E), while the siCtrl group had a negligible effect on TLR4 expression, indicating that Ad4-3 LNP systematically delivered siRNA to the peri-infarct region and silenced the key components in the transcription factor modulating pro-inflammatory response. To examine whether knockdown of TLR4 can alleviate secondary damage or inflammation in TBI mice, we measured the BBB integrity or permeability of TBI model mouse after knockdown TLR4 by systemically administration of Evans Blue dye (EB) to the Ad4-3 LNP-treated TBI mice. EB is one of the largest dyes commonly used for evaluation of BBB permeability due to its advantages of macroscopic observation and spectrophotometry quantification. EB cannot cross an intact BBB.[59] We i.v. injected EB dye to four groups of mice: sham group, PBS group, Ad4-3 LNP carrying siCtrl group, and Ad4-3 LNP carrying siTLR4 group (n = 6). The quantitative analysis revealed that EB content in the siTLR4 group was significantly decreased compared with the PBS group, indicating a good integrity of the BBB (Figure 4F). Therefore, it can be concluded that the destruction of the BBB can be alleviated after Ad4 LNP-mediated knockdown of TLR4 in astrocytes. Furthermore, the analysis of neuronal apoptosis by NeuN staining in brain tissue from the TBI mouse showed that the apoptosis of neurons near the brain injury area was significantly reduced in the siTLR4 group compared with the siCtrl group (Figure S10).

To investigate the change of cytokine expression pattern resulting from Ad4-LNP-mediated astrocyte-specific knockdown of TLR4 in mouse TBI models, we measured the serum level of representative cytokines involved in inflammatory immune response. TLR4 silencing results in significant changes in the expression characteristics of cytokines and other immune responders. The ELISA results showed that the expression levels of canonical pro-inflammation cytokines TNFα and IL-1β were dramatically decreased, while the anti-inflammation cytokines IL-4 and IL-13 were significantly upregulated (Figure 5), suggesting that RNAi-mediated TLR4 silencing possibly enabled transition of activated astrocytes from pro-inflammatory (A1) to anti-inflammatory (A2) phenotype at the injury site in the mouse TBI model.

In summary, LNP formulated from DoGo-derived ionizable lipid and adenosine-conjugated DoGo lipid can specifically deliver siRNA to astrocyte via AR-mediated internalization. Particularly, Ad4-3 LNP could specifically deliver siRNA in astrocytes in the peri-infarct region in the TBI mouse model, reprogram the polarization of astrocyte via knockdown TLR4, upregulate the expression of anti-inflammatory factors, and inhibit the secretion of pro-inflammatory factors, attenuating secondary neural damage in the mouse TBI model.

DISCUSSION

Neurological disorders are the second leading cause of death.[60] The development of drugs for CNS diseases is characterized by low treatment satisfaction, high demand for new drugs, and the lack of effective delivery systems, which deliver less than 1% of the dose to the brain in most cases, including trastuzumab.[61] However, systemic drug delivery to brain parenchyma can be achieved via receptor-mediated approaches, despite the tight junction of BBB. The receptors

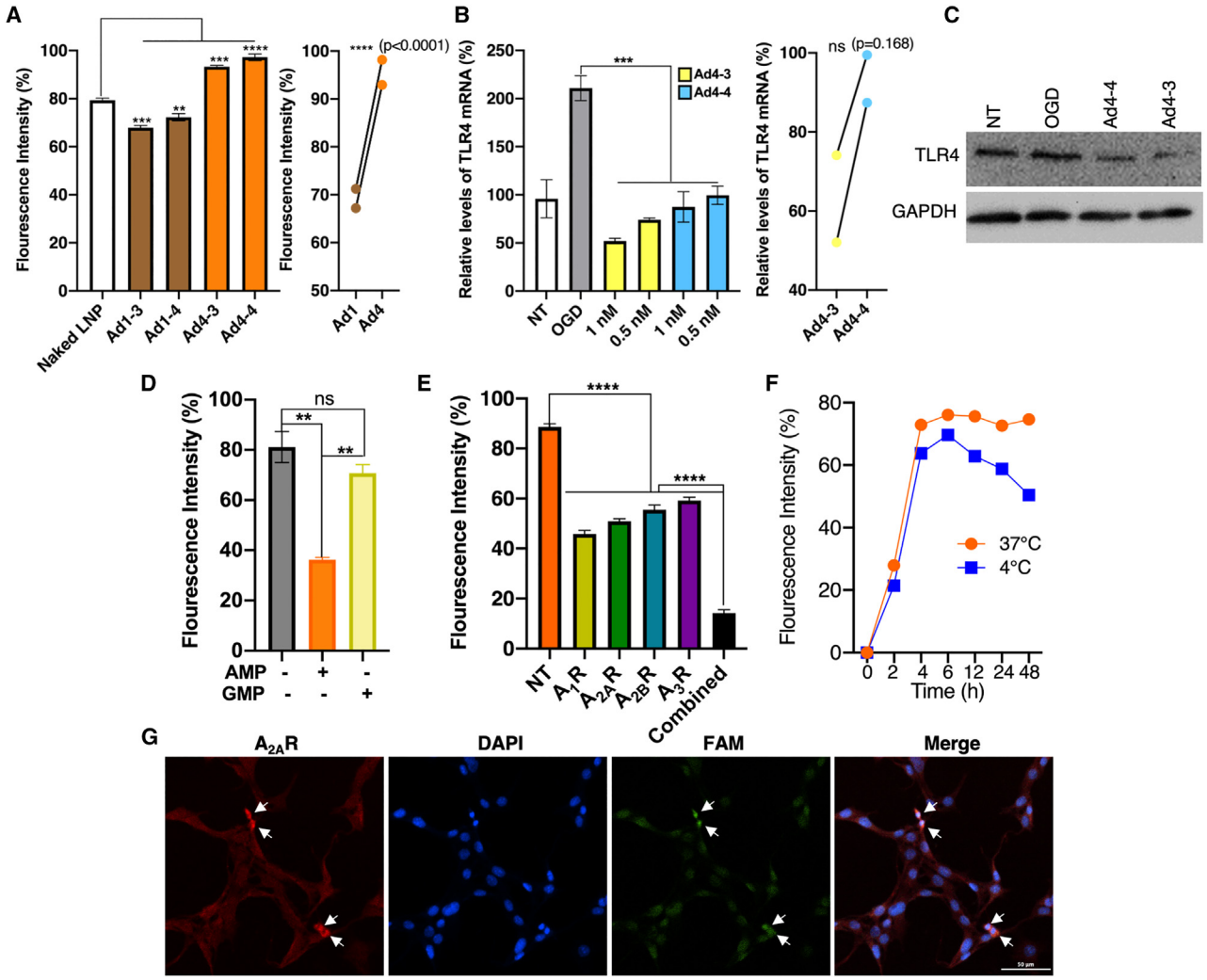

Figure 3. Ad4 LNP is internalized by astrocytes via adenosine receptors

(A) Cellular uptake of Ad1 and Ad4 LNP. C8-D1A cells were treated with Ad1-LNP (formulations 3 and 4) and Ad4-LNP (formulations 3 and 4) containing FAM-labeled siRNA, respectively. Twenty-four hours later, the fluorescence positive cells were quantitively analyzed by flow cytometry. (B) *In vitro* siRNA delivery efficiency of the Ad4-3 and Ad4-4 LNPs. OGD-treated C8-D1A cells were treated with Ad4-3 and Ad4-4 LNP containing siRNA against TLR4 (concentration: 1 nM and 0.5 nM), respectively. Twenty-four hours later, total RNA was extracted from the cells and the expression level of TLR4 was quantitively analyzed by RT-qPCR. (C) TLR4 protein levels in the siTLR4-treated cells were analyzed by western blot. (D) AMP competitively blocks the uptake of Ad4 LNP by C8-D1A cells. AMP but not GMP significantly reduces the internalization of Ad4 LNP carrying FAM-labeled siRNA. (E) Knockdown of adenosine receptors significantly reduces the uptake of Ad4 LNP by C8-D1A cells. (F) Uptake of Ad4 LNP by C8-D1A cells are temperature dependent. (G) Confocal images of C8-D1A cells treated with Ad4 LNP carrying FAM-labeled siRNA. Adenosine receptor positive cells (red) and FAM-labeled siRNA (green) are highly overlaying. Scale bar, 50 μm. **$p < 0.01$; ***$p < 0.001$; ****$p < 0.0001$.

on brain endothelial cells, such as transferrin receptors, insulin receptors, folate receptors, and low-density lipoprotein receptors have been utilized to study the systemic drug delivery efficiency of the ligand or antibody conjugated nanoparticles including LNPs in intact brain.[62] In the case of TBI patients, systemically delivered drugs may enter the brain parenchyma via impaired BBB at the site of injury. In this report, we synthesized four ionizable lipids based of our previously reported cationic lipids, i.e., DoGo lipids.[18] Because ionizable lipids are superior to the conventional cationic lipids in terms of RNA delivery, we used DEP-DoGo1 lipid in the formulation of ligand functionalized LNP for astrocyte targeting. Compared with the rest of the newly synthesized lipids, DEP-DoGo1-based LNP had the lowest pKa value and smallest particle size (Figure 1 and Table 1).

Astrocytes are the most abundant glial cells in the brain. In early stage of brain injury, astrocytes formulate the glial scar to isolate lesion zones and protect surviving cells and express growth factors and other molecules that can support the neuroregeneration.[63–65] However, astrocytes are also one of the major contributors to neuroinflammation, which is an important secondary injury mechanism that contributes

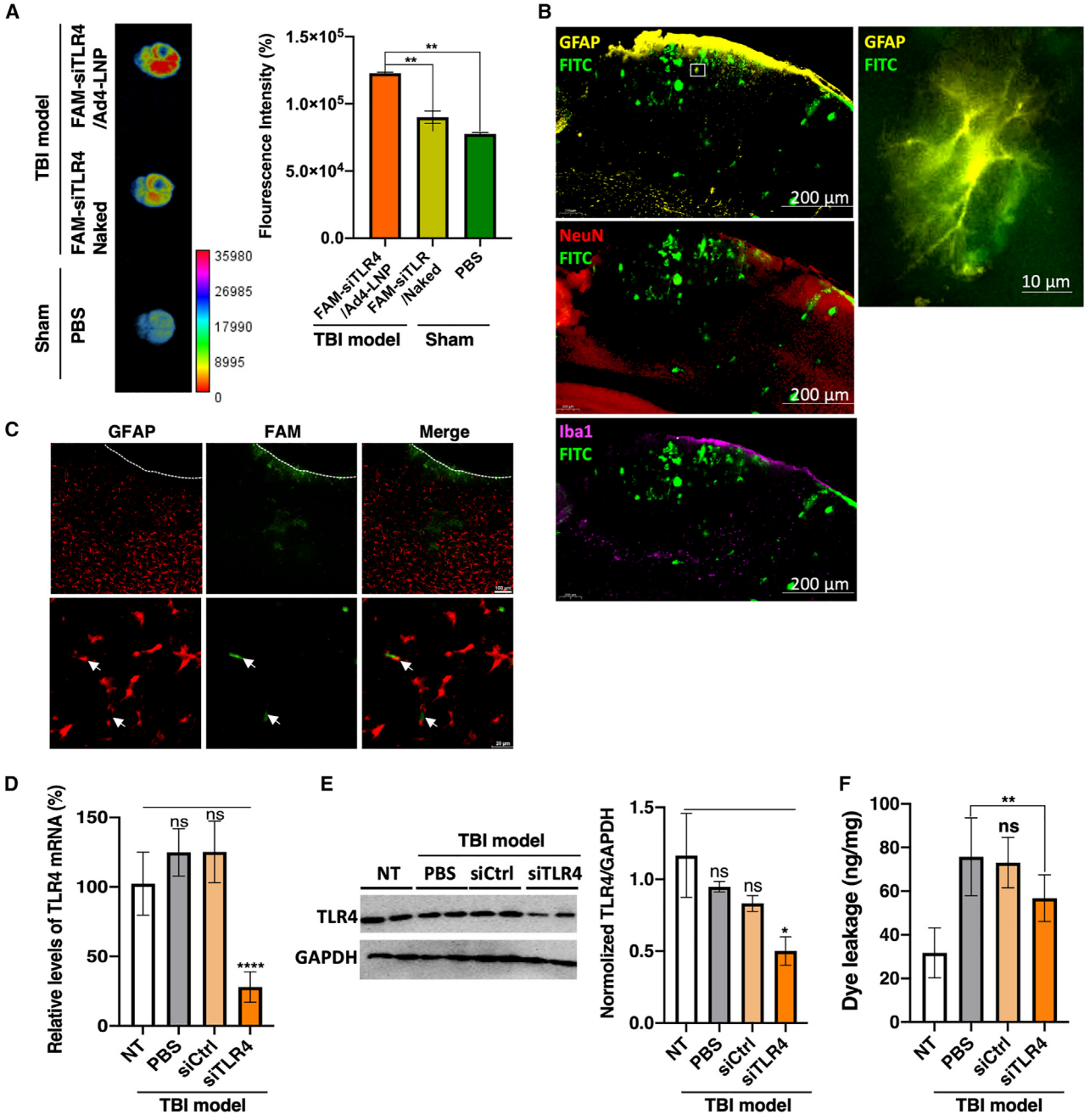

Figure 4. Astrocyte-specific siRNA delivery by Ad4 LNP in a TBI mouse model

(A) Images of mice brain harvested 24 h after administration of Ad4 LNP carrying FAM-labeled siRNA. TBI model mouse administered with naked siRNA and a sham-operated mouse injected with PBS are shown as control. (B) and (C) Confocal images of brain slides showing GFAP-positive cells at the boarder of damaged brain tissue colocalizing with FAM-labeled siRNA. (D) Quantification of TLR4 mRNA in the brain by RT-qPCR. (E) TLR4 protein level in the brain was analyzed by western blot. (F) Measurement of EB dye leakage in sham group, TBI model treated with PBS or Ad4 LNP carrying siCtrl or siTLR4, respectively; *$p < 0.05$; **$p < 0.01$; ***$p < 0.001$; ****$p < 0.0001$.

to ongoing neurodegeneration and neurological impairments associated with TBI.[66] Changing the glial cell phenotype and regulating cytokine expression may finally achieve the purpose of alleviating secondary brain injury after TBI incidence.[67] However, to the best of the authors' knowledge, no therapeutics have been reported to specifically target astrocytes. For example, Gal-NP@siRNA can penetrate the BBB via glycemia-controlled glucose transporter-1 (GLUT 1)-mediated transport, thereby ensuring that siRNAs decease BACE1

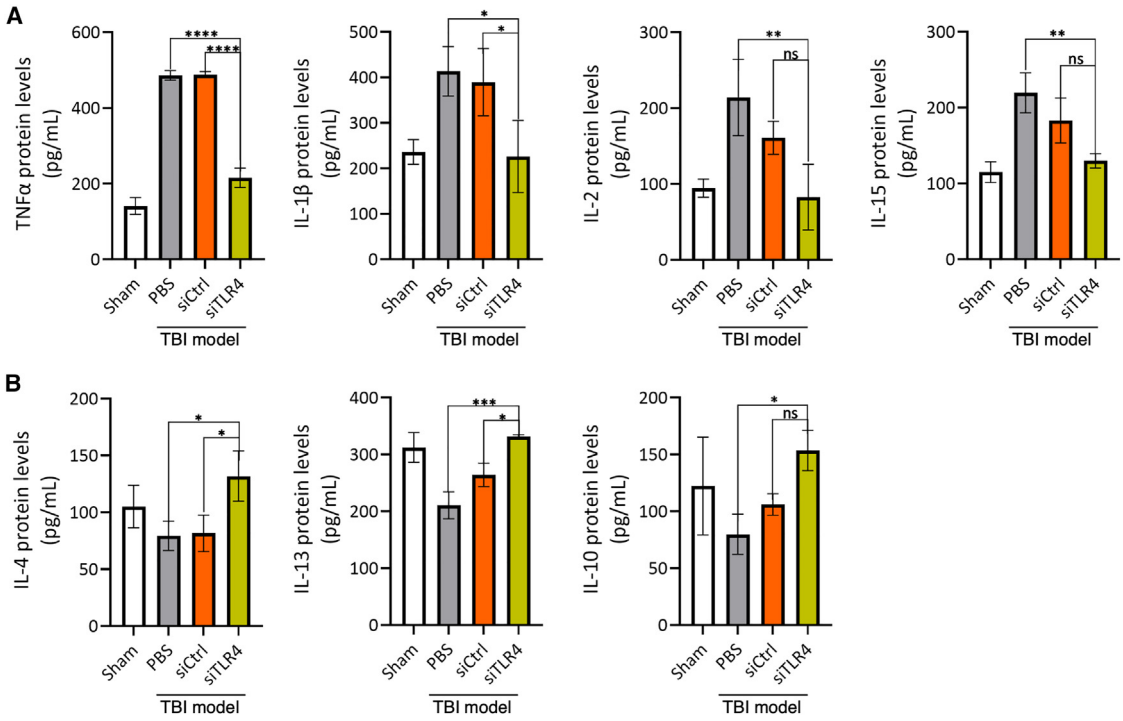

Figure 5. Ad4 LNP-mediated knockdown of TLR4 in astrocytes resulted in the down regulation of pro-inflammatory cytokines and upregulation of anti-inflammatory cytokines in mouse TBI model

ELISA measurement of serum cytokine level in sham group, PBS-treated group, Ad4 LNP group (carrying siCtrl and siTLR4, respectively). (A) Pro-inflammatory cytokines. (B) Anti-inflammatory cytokines. *p < 0.05; **p < 0.01; ***p < 0.001; ****p < 0.0001.

expression and modify relative pathways.[68] GLUT1 receptor-mediated NP can endocytose by brain capillary epidermal cells, neurons, and microglia, but not by astrocytes.

To explore the possibility of adenosine receptor-mediated siRNA delivery to astrocytes, we functionalized DoGo lipid by conjugating adenosine moieties and obtained Ad1-DoGo1 and Ad4-DoGo4 lipid (Figure 2). The advantages of ARs as the receptors for astrocyte-targeted siRNA delivery are as follows: (1) All four types of adenosine receptors (A1, A_{2A}, A_{2B}, and A3) are expressed by astrocytes.[69] (2) We previously proved that ARs can bind and facilitate the receptor-mediated internalization of adenosine-conjugated drug carriers.[51,70] (3) Our previous studies revealed that the adenosine-conjugated drug carriers are antagonistic to ARs and therefore exert immunosuppressive effects.[49,51] (4) Astrocytes are the major glial cells in the brain, making up 30% of the total glial cell population. TBI incidence induces the proliferation of astrocytes and increases the density of astrocytes in the infarct region, which reinforces the contribution of astrocytes during TBI-induced neuroinflammation process.[71] Therefore, astrocyte-specific delivery of therapeutics is crucial for the facilitation of the anti-inflammatory phenotype of the astrocyte population.

A side-by-side comparison revealed that Ad4-DoGo4 functionalized LNP (Ad4 LNP) was more efficient in terms of cellular uptake and *in vitro* RNAi activities on the C8-D1A cell line (Figures 3A and 3B). This may be attributed to the ligand density and clustering effect, which can greatly affect the efficiency of receptor-mediated siRNA delivery.[72] We proved that the internalization of Ad4 LNP was indeed dependent on AR by demonstrating the ligand blocking, receptor knockdown as well as temperature dependency experiments (Figures 3D–3G). Moreover, systemic administration of Ad4-LNP carrying dye-labeled siRNA in the TBI mouse model resulted in accumulation of siRNA at the injury site in the brain. Significantly, immunohistochemical analysis confirmed that the Ad4 LNPs were specifically taken up by GFAP-positive cells (Figure 4B), demonstrating the successful establishment of an astrocyte-specific RNA therapeutic delivery system. Remarkably, the robust knockdown of the target gene expression in the peri-infarct section of injured site (Figures 4A and 4B) led to the significantly decreased dye leakage in the brain (Figure 4E), which may have resulted from the BBB protective effect originated *in situ* from the phenotypically changed astrocytes at the vicinity of the injury site releasing the increased level of anti-inflammatory cytokines and decreased level of pro-inflammatory cytokines (Figure 4F).

The CNS of TBI mice is characterized by severe inflammatory responses induced by activated astrocytes and microglia, which also disrupt and increase permeability of the BBB. The cell debris resulting from TBI-induced neural cell apoptosis activates astrocytes via PRRs such as TLR4. Activation of the PRR pathway eventually facilitates nuclear localization of p65, initiates NF-κB-dependent transcription, expresses

pro-inflammatory cytokines including TNFα and IL-1β, and promotes pro-inflammatory polarization of astrocytes. TLR4 is widely distributed in the brain and plays a key role in neuroinflammation in the CNS. Therefore, it is a promising therapeutic target for clinical treatment of TBI.[73] The knockdown of TLR4 can deactivate the NF-κB pathway and subsequently induce neuroprotective ability.[74] In this paper, instead of analyzing the mechanism of the NF-κB pathway, we analyzed phenotypic polarization of astrocytes at the cytokine level. The results demonstrated that Ad4-3 LNP can weaken the NF-κB pathway signal through knockdown of TLR4, upregulate the expression of neuroprotective cytokines, and lead to neurovascular protection.

Astrocyte-specific delivery of RNA therapeutics potentiates a broad application of Ad LNP system for curing CNS disease. Further exploration of this unique system could include non-viral astrocyte-specific mRNA delivery for modulation of astrocyte-to-neuron conversion in neurodegenerative diseases. Overexpression of NeuroD1 by local injection of viral vector (AAV) in the brain showed limited astrocyte-to-neuron conversion, while systemic administration of increased doses of AAV may potentially increase the efficiency of this conversion and may also result in unintended broader expression.[75]

MATERIALS AND METHODS

Synthesis of ionizable lipids

SA-DoGo1

Succinic anhydride (SA, 1.24 mmol) was dissolved in dry dichloromethane (5 mL) under a nitrogen atmosphere with constant stirring at 35°C. Separately, the required DoGo1 (1.24 mmol) was dissolved in dry dichloromethane (5 mL) and added dropwise to the SA solution over a period of 5 min. The mixture was then heated at reflux for 5 h. After cooling to room temperature, the mixture was washed with 5% critic acid, distilled water, brine, and dried over anhydrous Na_2SO_4. The crude product was purified by chromatography silica gel using dichloromethane and methanol (v/v, 10/1) as eluent and the product (named SA-DoGo1, yield = 92%) dried under vacuum. ^{1}H NMR: 0.886–0.908 (t, 6 H, -CH_3), 1.289 (m, 44 H, -CH_2), 1.496–1.507 (m, 4 H, NHCH_2CH_2-), 1.931–2.031 (m, 8 H, -CH_2CH = CHCH_2-), 2.296–2.330 (m, 2 H, CO(NH)CHCH_2-), 2.536–2.593 (m, 2 H, CO(NH)CHCH_2CH_2-), 2.643–2.739 (m, 4 H, HOOCCH_2-, HOOCCH_2CH_2-), 3.206–3.253 (m, 4 H, CONHCH_2-), 4.431–4.466 (m, 1 H, CO(NH)CH-), 5.361–5.397 (m, 4 H, -CH_2 = CH_2-), 6.569 (t, 1 H, NH-), 7.205–7.223 (m, 1 H, NH-), 7.618–7.630 (d, 1 H, NH-). ^{13}C NMR: 14.093 (-CH_3), 22.670 (CH_3CH_2-), 27.219 (HOOCCH_2-, HOOCCH_2CH_2-), 28.693–28.860 (CO(NH)CHCH_2-, CO(NH)CHCH_2CH_2-), 31.898 (-CH_2CH = CHCH_2-), 39.841–39.965 (CONHCH_2-), 51.932 (CO(NH)CH-), 129.772–129.976 (-CH_2 = CH_2-), 171.660–173.540 (CO), 177.195 (CO). MS: Anal. Calcd for formula $C_{45}H_{83}N_3O_5$: 745.6333. Found: $(M + H)^+$, 746.6254.

DMB-DoGo1

SA-DoGo1 (300 mg, 0.4 mmol) was dissolved in dry dichloromethane (3 mL) under a nitrogen atmosphere with constant stirring at room temperature. Followed by the required 4-Dimethylamino-1-butanol (80 μL, 0.6 mmol), EDCI reagent (115 mg, 0.6 mmol), and DMAP catalyst were added. The reaction was continuously stirred overnight. Adding more dichloromethane, the mixture was washed with 5% citric acid, distilled water, and brine, and dried by anhydrous Na_2SO_4. The crude product was purified by silica gel chromatography using dichloromethane and methanol (5/1, v/v) as eluent and the product (named DMB-DoGo1, yield = 72%) dried under vacuum. ^{1}H NMR: 0.889–0.908 (t, 6 H, -CH_3), 1.269–1.361 (m, 44 H, -CH_2), 1.496–1.507 (m, 4 H, NHCH_2CH_2-), 1.681–1.722 (m, 2 H, -COOCH_2CH_2-), 1.853–2.125 (m, 12 H, -COOCH_2CH_2CH_2-, -CH_2CH = CHCH_2-, CO(NH)CHCH_2-), 2.336–2.413 (m, 2 H, CO(NH) CHCH_2CH_2-), 2.513–2.672 (m, 4 H, OOCCH_2-, OOCCH_2CH_2-), 2.720–2.752 (m, 6 H, -N(CH_3)$_2$), 2.843–2.951 (m, 2 H, -COOCH_2CH_2CH_2CH_2-), 3.170–3.252 (m, 4 H, CONHCH_2-), 4.101–4.162 (t, 2 H, COOCH_2-), 4.363–4.389 (m, 1 H, CO(NH)CH-), 5.333–5.412 (m, 4 H, -CH_2 = CH_2-), 6.389–6.409 (t, 1 H, NH-), 7.189–7.213 (m, 1 H, NH-), 7.632–7.640 (d, 1 H, NH-). ^{13}C NMR: 14.091 (-CH_3), 21.801 (COOCH_2CH_2CH_2-), 22.546–22.682 (CH_3CH_2-), 25.913(COOCH_2CH_2CH_2-), 26.962–27.001 (CO(NH)CHCH_2-), 27.118 (OOCCH_2-), 28.741–30.832 (CH_2-), 32.642 (-CH_2CH = CHCH_2-), 33.087 (CO(NH)CHCH_2CH_2-), 39.642–39.782 (CONHCH_2-), 43.578 (N(CH_3)$_2$), 52.752–53.143 (CO(NH)CH-), 57.942 (-COOCH_2CH_2CH_2CH_2-), 63.034 (COOCH_2-), 129.772–129.976 (-CH_2 = CH_2-), 171.240–172.970 (CO). MS: Anal. Calcd for formula $C_{51}H_{96}N_4O_5$: 844.7381. Found: $(M + H)^+$, 845.7427.

DEP-DoGo1

SA-DoGo1 (200 mg, 0.3 mmol) was dissolved in dry dichloromethane (3 mL) under a nitrogen atmosphere with constant stirring at room temperature. Followed by the required 3-Dimethylamino-1-propanol (81 μL, 0.6 mmol), EDCI reagent (104 mg, 0.6 mmol) and HOBt (73 mg, 0.6 mmol) were added. The reaction was continuously stirred overnight. Adding more dichloromethane, the mixture was washed with 5% citric acid, distilled water, brine, and dried by anhydrous Na_2SO_4. The crude product was purified by silica gel chromatography using dichloromethane and methanol (5/1, v/v) as eluent and the product (named DEP-DoGo1, yield = 75%) dried under vacuum. ^{1}H NMR: 0.853–0.913 (t, 6 H, -CH_3), 1.277–1.297 (m, 44 H, -CH_2), 1.388–1.412 (m, 6 H, NCH_2CH_3), 1.522 (m, 4 H, NHCH_2CH_2-), 2.013–2.121 (m, 12 H, -COOCH_2CH_2-, CH_2CH = CHCH_2-, CO(NH)CHCH_2-), 2.350–2.433 (m, 2 H, -COOCH_2CH_2-), 2.568–2.655 (m, 4 H, OOCCH_2-, OOCCH_2CH_2-), 3.165–3.252 (m, 10 H, CONHCH_2-, N(CH_2)$_2$-, CO(NH) CHCH_2CH_2-), 4.214–4.232 (t, 2 H, -COOCH_2-), 4.404–4.415 (m, 1 H, CO(NH)CH-), 5.354–5.374 (m, 4 H, -CH_2 = CH_2-), 6.340–6.352 (t, 1 H, NH-), 7.342–7.353 (m, 2 H, NH-). ^{13}C NMR: 8.791 (N(CH_2CH_3)$_2$), 14.091 (-CH_3), 22.671–29.773 (CH_2-), 30.721–31.892 (OOCCH_2-, OOCCH_2CH_2-), 32.602 (-CH_2CH = CHCH_2-), 32.951 (CO(NH)CHCH_2CH_2-), 39.652–39.788 (CONHCH_2-), 46.873 (N(CH_2)$_2$-), 48.832 (CO(NH)CH-), 53.162 (-COOCH_2CH_2CH_2-), 60.944 (COOCH_2-), 129.278–129.993 (-CH_2 = CH_2-), 171.190–173.083 (CO). MS: Anal. Calcd for formula $C_{52}H_{98}N_4O_5$: 858.7537. Found: $(M + H)^+$, 859.7551.

DME-DoGo1

SA-DoGo1 (200 mg, 0.3 mmol) was dissolved in dry dichloromethane (3 mL) under a nitrogen atmosphere with constant stirring at room

temperature. Followed by the required 2-Dimethylaminoethanol (55 μL, 0.6 mmol), EDCI reagent (104 mg, 0.6 mmol) and HOBt (73 mg, 0.6 mmol) were added. The reaction was continuously stirred overnight. Adding more dichloromethane, the mixture was washed with 5% critic acid, distilled water, brine, and dried by anhydrous Na_2SO_4. The crude product was purified by silica gel chromatography using dichloromethane and methanol (5/1, v/v) as eluent and the product (named DME-DoGo1, yield = 65%) dried under vacuum. ^{1}H NMR: 0.865–0.914 (t, 6 H, -CH_3), 1.091–1.280 (m, 44 H, -CH_2), 1.438 (m, 4 H, CONHCH$_2$CH$_2$-), 2.027–2.036 (m, 10 H, -CH_2CH = CHCH$_2$-, CO(NH)CHCH$_2$-), 2.229–2.254 (m, 2 H, CO(NH) CHCH$_2$CH$_2$-), 2.352–2.582 (m, 4 H, OOCCH$_2$-, OOCCH$_2$CH$_2$-), 2.659–2.768 (m, 6 H, N(CH_3)$_2$), 3.221–3.231 (m, 6 H, CONHCH$_2$-, COOCH$_2$CH$_2$-), 4.351–4.396 (t, 3 H, CO(NH) CH-, COOCH$_2$-), 5.366–5.400 (m, 4 H, -CH_2 = CH$_2$-), 6.294 (t, 1 H, NH-), 6.975 (t, 1 H, NH-), 7.612 (d, 1 H, NH-). ^{13}C NMR: 14.112 (-CH_3), 22.681–29.773 (CH_2-), 31.901–31.932 (CONHCH$_2$CH$_2$-), 39.692–39.788 (CONHCH$_2$-), 44.367–44.734 (N(CH_3)$_2$), 52.912–53.162 (-CO(NH)CH-), 56.805 (COO CH$_2$-, COOCH$_2$CH$_2$-), 129.787–129.963 (-CH_2 = CH$_2$-), 171.252–173.183 (CO). MS: Anal. Calcd for formula C49H92N4O5: 816.7068. Found: (M + H)$^+$, 817.7123.

DEE-DoGo1

SA-DoGo1 (200 mg, 0.3 mmol) was dissolved in dry dichloromethane (3 mL) under a nitrogen atmosphere with constant stirring at room temperature. Followed by the required diethylaminoethanol (72 μL, 0.6 mmol), EDCI reagent (104 mg, 0.6 mmol) and HOBt (73 mg, 0.6 mmol) were added. The reaction was continuously stirred overnight. Adding more dichloromethane, the mixture was washed with 5% critic acid, distilled water, brine, and dried by anhydrous Na_2SO_4. The crude product was purified by silica gel chromatography using dichloromethane and methanol (5/1, v/v) as eluent and the product (DEE-DoGo1, yield = 63%) dried under vacuum. ^{1}H NMR: 0.891–0.913 (t, 6 H, -CH_3), 1.293–1.390 (m, 50 H, N(CH$_2$CH$_3$)$_2$, -CH_2), 1.514 (m, 4 H, CONHCH$_2$CH$_2$-), 2.025–2.034 (m, 10 H, -CH_2CH = CHCH$_2$-, CO(NH)CHCH$_2$-), 2.323–2.433 (m, 2 H, CO(NH)CHCH$_2$CH$_2$-), 2.562–2.741 (m, 4 H, OOCCH$_2$-, OOCCH$_2$CH$_2$-), 3.220–3.334 (m, 10 H, COOCH$_2$CH$_2$-, N(CH_2)$_2$-, CONH(CH_2)-), 4.355–4.498 (m, 3 H, CO(NH)CH-, COOCH$_2$-), 5.365–5.400 (m, 4 H, -CH_2 = CH$_2$-), 6.465 (t, 1 H, NH-), 7.108–7.128 (t, 1 H, NH-), 7.632 (d, 1 H, NH-). ^{13}C NMR: 9.002 (N(CH$_2$CH$_3$)$_2$), 14.112 (-CH_3), 22.673 (CH$_3$CH$_2$-), 26.934–26.982 (CO(NH)CHCH$_2$-), 27.222–29.943 (CH_2-), 31.941 (OCOCH$_2$-, OCOCH$_2$CH$_2$-), 32.601–39.988 (-CH_2CH = CHCH$_2$-), 39.687–39.823 (CONH(CH_2)-), 47.405 (N(CH_2)$_2$-), 50.633–50.812 (-CO(NH)CH-, COOCH$_2$CH$_2$-), 52.985 (COOCH$_2$-), 129.757–129.967 (-CH_2 = CH$_2$-), 171.142–173.118 (CO). MS: Anal. Calcd for formula $C_{51}H_{96}N_4O_5$: 844.7381. Found: (M + H)$^+$, 845.7665.

Synthesis of adenosine-conjugated lipids

Ade 1

Compound 1. A suspension of 2′,3’-(isopropylidene) adenosine (200 mg, 0.65 mmol), hexamethyldisilazane (HMDS; 271 μL), and 4-dimethylaminopyridine (DMAP; 16 mg) was magnetically stirred at 25°C. Trimethylsilyl trifluoromethanesulfonate (TMSOTf; 24 μL) was dropwise added to above suspension, then further 2 h at 75°C. The mixture was evaporated to oil that was dissolved in 3 mL dry THF and treated with di-t-butyl dicarbonate (449 mg; 1.95 mmol) and DMAP (8 mg) in an ice bath, then stirred at 25°C for 4 h. The solution was concentrated and then treated with 6 mL of 5:1 (v/v) methanol:triethylamine. The reaction was performed at 55°C for 16 h and then evaporated to oil, the remaining mixture was taken up in dichloromethane. The organic phase was concentrated and purified by silica gel chromatography using ethyl acetate and hexane (5/1, v/v) as eluent, Rf = 0.2. Combined product fractions were concentrated to an oil that was pumped in vacuo 50°C to leave compound 1 (296 mg, yield: 90%). ^{1}H NMR: 1.348–1.394 (d, 24 H, -COOC(CH_3)$_3$, C(CH_3)$_2$), 3.520–3.545 (m, 2 H, -CH_2OH), 4.283–4.289 (q, 1 H, -CH(CH-O-)-O-), 4.993–5.010 (t, 1 H, -OH), 5.090–5.111 (t, 1 H, -CH(CH-O-)-O-), 5.443–5.460 (m, 1 H, -CH(O)CH$_2$OH), 6.287–6.293 (d, 1 H, -O-CH(N)-), 8.816 (s, 1 H, -N=CH-N =), 8.881 (s, 1 H, -N=CH-N). ^{13}C NMR: 25.625 (-CH_3), 27.458–27.768 (-COO C(CH_3)$_3$), 61.885 (-CH_2OH), 81.864 (-CH(CH-O-)-O-), 83.925–84.063 (-COOC(CH_3)$_3$), 87.569 (-CH(CH-O-)-O-), 90.574 (-CH(O)-CH_2OH), 113.527 (-O-CH(N)-), 128.561 (-(O)C(CH_3)$_2$), 132.251 (-N(N)C=C(N =)-), 145.690 (-N=CH-N), 149.777 (-N=C(N)-), 150.459 (-COOC(CH_3)$_3$), 152.198 (N=C(N =)-), 152.903 ((Boc)$_2$N-C(=C)-). MS: Anal. Calcd for formula $C_{23}H_{33}N_5O_8$: 507.2329. Found: (2 M + Na)$^+$, 1037.4720.

Compound 2. Compound 1 (200 mg, 0.395 mmol) was dissolved in dry dichloromethane, to this 4-dimethylaminopyridine (DMAP; 97 mg) was added and added dropwise a solution of 4-nitrophenyl chloroformate (159 mg, 0.79 mmol). The mixture was stirred at room temperature under nitrogen atmosphere overnight. The extra solvent was removed by evaporation, and purified by silica gel chromatography using petroleum and ethyl acetate (2/1, v/v) as eluent, Rf = 0.3. The product fractions were concentrated to oil that was dried in vacuo at 50°C to get compound 2 (228 mg, 86% yield). ^{1}H NMR: 1.163–1.587 (d, 24 H, -COOC(CH_3)$_3$, C(CH_3)$_2$), 4.393–4.429 (q, 1 H, -CH(CH-O-)-O-), 4.506–4.580 (m, 2 H, -CH_2OH), 5.193–5.212 (t, 1 H, -CH(CH-O-)-O-), 5.543–5.560 (m, 1 H, -CH(O)CH$_2$OCO), 6.397–6.500 (d, 1 H, -O-CH(N)-), 7.448–7.473 (m, 2 H, -CH = C(NO_2)-, 8.255–8.287 (m, 2 H, -HC = C(C=C)-), 8.824 (s, 1 H, -N=CH-N =), 8.888 (s, 1 H, -N=CH-N). ^{13}C NMR: 25.675 (-CH_3), 27.394–27.733 (-COO C(CH_3)$_3$), 68.730 (-CH_2OH), 81.225 (-CH(CH-O-)-O-), 83.792–84.275 (-COOC(CH_3)$_3$, -CH(O)CH$_2$OCO), 90.218 (-CH(CH-O-)-O-), 114.116 (-O-CH(N)-), 122.857 (-HC = C(C=C)-), 125.769 (m, 2 H, -CH = C(NO_2)-), 128.671 (-N(N)C=C(N =)-, -(O)C(CH_3)$_2$), 145.644–145.956 (-N=CH-N, C=C(NO_2)-), 149.883–150.462 ((Boc)$_2$ N-C(=C)-, -COOC(CH_3)$_3$), 152.033–152.754 (-N=C(N)-, -OCOO-, -N=CH-N =), 155.570 (OCOO-C(C =) = C)). MS: Anal. Calcd for formula $C_{30}H_{36}N_6O_{12}$: 672.2391. Found: (2 M + Na)$^+$, 1367.4766.

Compound 3. To a solution of compound 2 (200 mg, 0.30 mmol) in dry dichloromethane (2 mL) was added a solution of Val-DoGo1 (335 mg, 0.45 mmol) in dry dichloromethane, followed by N,N-diisopropylethylamine (DIPEA, 75 mL). The reaction mixture was stirred at room temperature under nitrogen atmosphere for 24 h. The extra

solvent was removed and purified by flash chromatography, eluting with dichloromethane and methanol (15/1, v/v) to give compound 3 (306 mg, 80% yield), Rf = 0.5. ^{1}H NMR: 0.836–0.862 (t, 6 H, -CH_3), 1.234–1.650 (m, 76 H, -$COOC(CH_3)_3$, CH_2, OCONH CH_2CH_2-, $OCONHCH_2CH_2CH_2$-, -$(O)C(CH_3)_2$), 1.708–2.112 (m, 14 H, -CH_2CH = $CHCH_2$-, NHCOCH(NH)CH_2-, NHCOCH(NH) CH_2CH_2-, $OCONHCH_2CH_2CH_2CH_2$-), 2.903–3.064 (m, 6H, $OCONHCH_2$-, $CH_2CONHCH_2$-, $CHCONHCH_2$-), 3.979–4.016 (m, 1 H, -CH(NH)CO), 4.132–4.177 (m, 2 H, -CH_2OCO-), 4.386–4.414 (q, 1 H, -CH(CH-O-)-O-), 5.028–5.045 (t, 1 H, -CH(CH-O-)-O-), 5.308–5.349 (m, 4 H, -H_2C = CH_2-), 5.540–5.557 (m, 1 H, -CH(CH)CH_2O-), 6.325–6.330 (d, 1 H, -O-CH(CH)N), 7.185–7.207 (t, 1 H, -NH-), 7.691–7.760 (m, 3 H, -NH-), 8.770 (s, 1 H, -N=CH-N =), 8.885 (s, 1 H, -N=CH-N). ^{13}C NMR: 14.356 (-CH_3), 22.520–22.958 (-$(O)C(CH_3)_2$), 25.637–27.434 (-CH_2), 27.747–27.924 (-$COOC(CH_3)_3$), 28.877–29.603 (-CH_2), 31.716 (NHCOCH (NH)CH_2CH_2-), 32.371 (-CH_2CH = $CHCH_2$-), 35.221 (OCONH $CH_2CH_2CH_2CH_2$-), 38.863–38.908 ($OCONHCH_2$-, CH_2CONHC H_2-), 52.716 (-CH(NH)CO), 64.047 (-CH_2OCO-), 81.745 (-CH(CH-O-)-O-), 83.679–83.917 (-CH(CH)CH_2O-, -$COOC(CH_3)_3$), 90.101 (-CH(CH-O-)-O-), 113.955 (-O-CH(CH)N), 130.074–130.511 (-N (N)C=C(N =)-, -H_2C = CH_2-, -$(O)C(CH_3)_2$), 145.649 (-N=CH-N), 149.894–150.413 (-N=C(N)-, -$COOC(CH_3)_3$), 152.279–152.818 ($(Boc)_2$N-C(=C)-, -N=CH-N =), 156.008 (OCO-), 171.564–171.682 (-NHCO-), 172.339 (-NHCO-). MS: Anal. Calcd for formula $C_{70}H_{119}N_9O_{12}$: 1277.8978. Found: $(M + Na)^+$, 1300.6721.

Ade 1. To a solution of compound 3 in dichloromethane (3 mL) was added trifluoroacetic acid (TFA; 3 mL). The mixture was stirred at room temperature for 4 h, the progress of the reaction was detected by thin-layer chromatography (TLC). After completion of the reaction, the solution was concentrated and washed with dichloromethane to obtain target compound Ade 1. ^{1}H NMR: 0.836–0.861 (t, 6 H, -CH_3), 1.052–1.506 (m, 48 H, -CH_2-), 1.629–1.824 (m, 4 H, $OCONHCH_2CH_2$-, $OCONHCH_2CH2CH_2$-), 1.912–2.127 (m, 14 H, -CH_2CH = $CHCH_2$-, NHCOCH(NH)CH_2-, NHCOCH(NH) CH_2CH_2-, $OCONHCH_2CH_2CH_2CH_2$-), 2.923–3.084 (m, 6H, $OCONHCH_2$-, $CH_2CONHCH_2$-, $CHCONHCH_2$-), 4.076–4.251 (m, 6 H, -CH(NH)CO, OH, -CH_2OCO-, -CH(CH-O-)-O-), 4.629–4.651 (t, 1 H, -CH(CH-O-)-OH), 5.046 (m, 1 H, -CH(CH)CH_2O-), 5.306–5.359 (m, 4 H, -H_2C = CH_2-),5.925–5.937 (d, 1 H, -O-CH(CH)N), 7.267 (t, 2 H, -NH_2), 7.698–7.851 (m, 4 H, -NH-), 8.269 (s, 1 H, -N=CH-N =), 8.423–8.436 (s, 1 H, -N=CH-N). ^{13}C NMR: 14.336 (-CH_3), 22.516–22.991 (-CH_2), 24.754 (NH(CH) CH_2-), 25.604 (NH(CH)CH_2CH_2-), 26.773–27.406 ($CH_3CH_2CH_2$-), 28.913–29.540 (-CH_2CH = $CHCH_2$-), 31.626–31.714 (NHC OCH(NH)CH_2CH_2-), 32.259 ($CH_2CONHCH_2$-), 35.234 (NH(CH) $CONHCH_2$-), 38.982 ($OCONHCH_2$-), 52.738 (-CH(NH)CO), 64.111–64.335 (-CH_2OCO-), 71.004 ((-CH(CH-O-)-OH), 73.920 ((-CH(CH-O-)-OH), 80.833 (-CH(CH)CH_2O-), 90.148 (-O-CH(CH)N), 119.260–119.430 (-N(N)C=C(N =)-), 130.064–130.502 (-H_2C = CH_2-), 141.761–141.999 (-N=CH-N), 147.498–149.244 (-N=C(N)-), 152.116 (-N=CH-N =), 158.414–159.704 (H_2N-C(=C)-), 158.995–159.284 (-NHCO-), 171.595–171.725 (-NHCO-). MS: Anal. Calcd for formula $C_{57}H_{99}N_9O_8$: 1037.76. Found: $(M + C_2H_3N)^+$, 1079.10.

Ade 4

Compound 1. DoGo1 (200 mg, 0.310 mmol) was dissolved in dry dimethyl formamide (DMF), followed by adding a solution of Di-Boc-Osu (160 mg, 0.372 mmol) and N,N-diisopropylethylamine (DIPEA, 62 μL). The mixture was stirred at room temperature under nitrogen atmosphere overnight. The extra solvent was removed by evaporation, and washed with water and brine. The organic layer was dried (Na_2SO_4), concentrated, and purified by silica gel chromatography using dichloromethane and methanol (10:1) as eluent. To a solution of Di-Boc-DoGo1 in dichloromethane (3 mL) was added trifluoroacetic acid (TFA; 3 mL). The mixture was vigorously stirred at room temperature for 30 min. The product fractions were concentrated to oil that was dried in vacuo at 50°C to obtain compound 1 (210 mg, 89% yield). ^{1}H NMR: 0.852–0.856 (t, 6 H, -CH_3), 1.236–1.371 (m, 68 H, $OCONHCH_2CH_2$-, -CH_2-, COOC $(CH_3)_3$), 1.687 (d, 2 H, NHCHCH_2-), 1.938–2.028 (m, 12 H, -CH_2CH = $CHCH_2$-, $NHCOCH_2$-, $NHCOCH_2CH_2$-), 2.883–3.049 (d, 4 H, $CONHCH_2$-), 3.843 (d, 2 H, NHCOCH(NH)-), 4.122 (d, 2 H, NHCOCH(NH)-), 5.321 (m, 4 H, -CH_2 = CH_2-), 6.787 (m, 1 H, OCONH(CH_2)-), 7.055 (m, 1 H, OCONH(CH)-), 7.726 (m, 1 H, $CONH(CH_2)$-), 8.080–8.090 (m, 2 H, (CH)CONH(CH)-, (CH)CO $NH(CH_2)$-). ^{13}C NMR: 14.404 (-CH_3),22.559–29.606 (-CH_2-, COO $C(CH_3)_3$), 31.747 (-CH_2CH = $CHCH_2$-), 38.903–38.976 (-Boc $NHCH_2$-, $CONHCH_2$-), 52.719 (-NHCOCH(NHBoc)-), 54.857 ($NHCOCH(CH_2)$-), 77.815–78.650 ($COOC(CH_3)_3$), 130.090–130.533 (-CH_2 = CH_2), 156.026–156.127 ($COOC(CH_3)_3$), 171.172–172.669 (-CO). MS: Anal. Calcd for formula $C_{56}H_{105}N_5O_7$: 959.8014. Found: $(M + Na)^+$, 984.0798.

Compound 2. Compound 1 (200 mg, 0.263 mmol) was dissolved in dry DMF, followed by adding Di-Boc-Osu (249 mg, 0.579 mmol) and N,N-diisopropylethylamine (DIPEA, 96 μL). The mixture was stirred at room temperature under nitrogen atmosphere overnight. The extra solvent was removed by evaporation, and washed with water and brine. The organic layer was dried (Na_2SO_4), concentrated, and purified by silica gel chromatography using dichloromethane and methanol (10:1) as eluent. To a solution of 4-Boc-DoGo1 in dichloromethane (3 mL) was added trifluoroacetic acid (TFA; 3 mL). The mixture was vigorously stirred at room temperature for 30 min. The product fractions were concentrated to oil that was dried in vacuo at 50°C to obtain compound 2 (232 mg, 90% yield). ^{1}H NMR: 0.853 (t, 6 H, -CH_3), 1.236–1.368 (m, 96 H, $OCONHCH_2CH_2$-, -CH_2-, $COOC(CH_3)_3$), 1.978–2.029 (m, 12 H, -CH_2CH = $CHCH_2$-, $NHCOCH_2$-, $NHCOCH_2CH_2$-), 2.507–3.033 (t, 10 H, $CONHCH_2$-), 3.838–3.897 (t, 2 H, NHCOCH(NH)-), 4.146–4.249 (t, 2 H, NHCOCH(NH)-), 5.320 (m, 4 H, -CH_2 = CH_2-), 6.767–6.865 (m, 4 H, OCONH(CH_2)-), 7.749–7.957 (m, 4 H, $CONH(CH_2)$-, (CH)CONH(CH_2)-), 8.111 (d, 1 H, (CH)CONH(CH)-). ^{13}C NMR: 14.404 (-CH_3),22.559–29.606 (-CH_2-, $COOC(CH_3)_3$), 31.747 (-CH_2 CH = $CHCH_2$-), 38.903–38.976 (-BocNHCH$_2$-, $CONHCH_2$-), 52.719 (-NHCOCH(NHBoc)-), 54.857 ($NHCOCH(CH_2)$-), 77.815–78.650 ($COOC(CH_3)_3$), 130.090–130.533 (-CH_2 = CH_2), 156.026–156.127 ($COOC(CH_3)_3$), 171.172–172.669 (-CO).

Compound 3. Compound 2 (200 mg, 0.202 mmol) was dissolved in dry dichloromethane, and added N,N-diisopropylethylamine (DIPEA, 167 μL), followed by adding dropwise a solution of Ade 1-compound 2 (681 mg, 1.012 mmol). The mixture was stirred at room temperature under nitrogen atmosphere overnight. The extra solvent was removed by evaporation, and washed with water and brine. The organic layer was dried (Na_2SO_4), concentrated, and purified by silica gel chromatography using dichloromethane and methanol (8:1) as eluent. ^{1}H NMR: 0.833–0.844 (t, 6 H, -CH_3), 1.216–1.556 (m, 156 H, OCONHCH_2CH_2-, OCONHCH_2CH_2CH_2-, NHCOCH_2-, NHCOCH_2CH_2-, -CH_2-, C(CH_3)$_2$-, COOC(CH_3)$_3$), 1.913–1.556 (m, 12 H, -CH_2CH = CHCH_2-, NHCOCH_2-, NHCOCH_2CH_2-), 2.896–3.046 (m, 10 H, CONHCH_2-), 3.938–4.383 (m, 16 H, -CH(CH-O-)-O-, -CH_2OC-ONH), 5.034 (t, 4 H, NHCOCH(NH)-), 5.312–5.344 (m, 4 H, -CH(O)CH_2OCO), 5.545 (m, 4 H, -CH_2 = CH_2-), 6.333 (m, 4 H, -O-CH(N)-), 6.888–6.901 (t, 1 H, OCONH(CH_2)-), 7.221–7.255 (t, 1 H, OCONH(CH_2)-), 7.431–7.444 (d, 2 H, OCONH(CH)-), 7.759–8.118 (t, 5 H, CHCONH-, CONH(CH_2)-), 8.787–8.818 (s, 4 H, N=CH-N =), 8.892 (s, 4 H, -N=CH-N). ^{13}C NMR: 14.366 (-CH_3), 22.526 (CH_3CH_2-), 25.616 (OCONHCH_2CH_2-, CHCONHCH_2CH_2-), 26.779–29.538 (NHCOCH_2CH_2-, CH_3CH_2CH_2-, NHCOCH_2-, C(CH_3)$_2$, -CH_2), 31.718 (-CH_2CH = CHCH_2-), 38.865–39.081 (OCONHCH_2-, CONHCH_2-), 63.570–64.077 (-CH_2OCONH, -(CH_2)CHNH(CH_2), -(CH_2)CHNH(CO)), 83.657–83.934 (-CH(CH-O)-O-, -(COO)C(CH_3)$_2$), 90.202–90.423 (-CH(O)CH_2OCO), 104.365 (-CH(CH-O)-O-), 116.289 (-O-CH(N)-), 126.655 (-(CH_3)$_2$C(O)$_2$), 128.615 (-C(C)=(N)-N(Boc)$_2$), 130.075 (CH_2 = CH_2), 140.3 (-N=CH-N), 150.032–150.418 (N=CH-N = , -N=C(N)-), 152.307–152.822 (C=O), 172.610–173.206 (C=O).

Ade 4. To a solution of compound 3 in dichloromethane (3 mL) was added trifluoroacetic acid (TFA; 3 mL). The mixture was stirred at room temperature for 4 h, the progress of the reaction was detected by TLC. After the completion of the reaction, the solution was concentrated and washed with dichloromethane to obtain target compound Ade 4 (350 mg, 80% yield). ^{1}H NMR: 0.836–0.858 (t, 6 H, -CH_3), 1.230–1.643 (m, 60 H, -CH_2-), 1.930–2.026 (m, 12 H, -CH_2CH = CHCH_2-, NHCOCH_2-, NHCOCH_2CH_2-), 2.984–3.083 (m, 10 H, CONHCH_2-), 4.002–4.341 (m, 16 H, -CH(CH-O-)-O-, -CH_2OCONH), 4.999 (t, 4 H, NHC OCH(NH)-), 5.316–5.346 (m, 4 H, -CH(O)CH_2OCO), 5.442 (m, 4 H, -CH_2 = CH_2-), 6.194–6.205 (m, 4 H, -O-CH(N)-), 6.933–8.134 (m, 17 H, -NH, -NH_2), 8.261–8.291 (s, 4 H, N=CH-N =), 8.379–8.407 (s, 4 H, -N=CH-N). ^{13}C NMR: 14.349 (-CH_3), 22.511 (CH_3CH_2-), 25.612 (OCOCH_2CH_2-), 26.807–27.420 (CONHCH_2CH_2CH_2-, NHCOCH_2-), 29.019–29.582 (OCOCH_2CH_2CH_2-, CONH(CH_2)$_3$CH_2-CONH(CH_2)$_4$ CH_2-, CONH(CH_2)$_5$CH_2-, CONH(CH_2)$_6$CH_2-, CH_3CH_2CH_2-, CH_3 (CH_2)$_2$CH_2-, CH_3(CH_2)$_3$CH_2-, CH_3(CH_2)$_4$CH_2-, CONHCH_2CH_2-), 31.706 (NHCOCH_2-, -CH_2CH = CHCH_2-), 52.657 (OCOCH_2-), 64.723–64.051 (-(CH_2)CHNH(CH_2), -(CH_2)CHNH(CO)), 73.683 (-CH_2OC-ONH), 81.770 (-CH(CH-O)-O-), 83.777–84.439 (-CH(CH-O)-O-), 87.732–88.089 (-CH(O)CH_2OCO), 89.763 (-O-CH(N)-, 116.255 (-C(C) =(N)-NH_2), 130.055 (CH_2 = CH_2), 141.067 (-N=CH-N), 149.057 (-N=C(N)-), 150.062–151.112 (N=CH-N =), 156.221 (NH_2-C(=C)-), 158.577–158.853 (C=O), 170.909–172.212 (C=O). MS: Anal. Calcd for formula $C_{100}H_{153}N_{29}O_{25}$: 2160.1592. Found: (M - H)$^-$, 2158.9636.

LNP formulation and characterization

For the preparation of LNPs, the desired lipids and siRNA were dissolved in 95% ethanol and 50 mM citrate buffer (pH = 5.0), respectively. The ethanol solution of lipids contained DoGo-derived ionizable lipid (DMB-, or DEP-, or DME-, or DEE-DoGo1), the helper lipid (DSPC), cholesterol, and DGM-PEG_{2000} in a molar ratio of 50:10:38.5:1.5. Equal volumes of lipid solution and siRNA solution (50 nM) were mixed and diluted into an equal volume of 50 mM citrate buffer (pH = 6.0). The mixture was repeatedly extruded through a 30-μm membrane (Avanti Polar Lipids, Inc., AL, USA). Then, the lipid complexes were dialyzed in a 10 KMWCO slide-A-Lyzer mini dialysis device (Thermo Fisher Scientific, MA, USA) overnight against 1x DPBS (pH = 7.4) at 4°C to remove ethanol.

The morphology of the LNPs was characterized by TEM (FEI, 80 kV, USA). The mean diameter and zeta potentials of the LNPs after dialysis was determined by dynamic light scattering (Malvern Zetasizer Nano instrument, Malvern, UK). Lipid concentrations and encapsulation efficiency (EE) were assessed by measuring the concentration of unencapsulated siRNA in LNPs. Briefly, the LNPs containing FAM-labeled siRNA after dialysis were centrifuged at 15,000 rpm for 10 min, and the supernatant fluorescence intensity (Ex/Em = 480/520 nm) was measured using FilterMax F5 Multi-Mode Microplate Reader (Molecular devices, CA, USA). The calculation formula was EE (%) = $(F_0 - F_1)/F_0 \times 100\%$, where F_0 and F_1 were the fluorescence intensity of siRNA used for LNP formulations and in the supernatant, respectively. The pKa of each ionizable lipid formulation was determined by TNS binding assay described previously.[54]

The stability of lipid in full medium was investigated as follows: DEP-DoGo1 was dissolved in ethanol to a final concentration of 4 mg/mL; 5 μL of DEP-DoGo1 ethanol solution was added to 20 μL full medium (DMEM medium containing 10% fetal bovine serum) and mixed thoroughly. After incubating the mixture at room temperature for 0, 1, 2, and 3 days, the concentration of DEP-DoGo1 in each incubation was measured by TLC using dichloromethane (DCM) and methanol (10:1 volume ratio) as the eluent. The lipid spots on the TLC plate were visualized using iodine vapor. The ethanol solution of DEP-DoGo1 and the full medium were used as control. and the results were quantified by ImageJ software.

To prepare Ad LNPs, Ad1-DoGo1 or Ad4-DoGo4 was mixed with DEP-DoGo1, cholesterol, DSPC, and DMG-PEG_{2000} at the required molar ratio (Table S2), respectively, and dissolved in 95% ethanol. Then, the ethanol solution and critic acid (pH = 5.0) solution of siRNA (50 nM) were mixed thoroughly at equal volumes, then diluted by an equal volume of 50 mM citrate buffer (pH = 6.0). The mixture was repeatedly extruded through a 30-μm membrane (Avanti Polar Lipids, Inc., AL, USA). The lipid complexes were dialyzed in 10 KMWCO slide-A-Lyzer mini dialysis device (Thermo Fisher Scientific, MA, USA) overnight against 1xDPBS (pH = 7.4) in 4°C.

Analysis of cellular uptake efficiency of LNPs

Cellular uptake of Ad LNPs carrying FAM-labeled siTLR4 and subsequent RNAi effect were monitored *in vitro* on a C8-D1A cell line. Cells were plated in 12-well plates at 2.5×10^5 cells per well density and incubated overnight before transfection of the LNPs. After transfection for 4 h, cellular uptake efficiency was examined by flow cytometry. For OGD insult,[76] cells were cultured in low glucose DMEM in incubation chamber with 5% CO_2, and 95% N_2 for 2 h and further incubated in high glucose medium to reoxygenate for 24 h under normal conditions. The total RNA was extracted with TRIzol (Invitrogen, Carlsbad, CA, USA) and the expression of endogenous TLR4 mRNA was measured using iScript reverse transcription supermix for RT-qPCR and iTaq Universal SYBR Green supermix (Bio-Rad, Hercules, CA, USA) for qPCR.

Receptor blocking and temperature-dependent cellular uptake

In brief, C8-D1A cells were seeded in a 24-well plate at a density of 1×10^6 cells per well and cultured for 24 h. Then the cells were treated with AMP (90 μg/mL) for 2 h, followed by addition of Ad4-3 LNP containing FAM-labeled siTLR4. After further incubation for 6 h, FAM-positive cells were quantified by flow cytometry. For antisense oligonucleotide (ASO)-mediated knockdown of AR receptors, ASO against A_1R, $A_{2A}R$, $A_{2B}R$, and A_3R, or a mixture of four ASO sequences (100 μM) was transfected into C8-D1A cells by DoGo4 transfection reagent, respectively, and the knockdown efficiency was confirmed by RT-qPCR. After 24 h, Ad4-3 LNP carrying FAM-labeled siRNA was added to the cells for 6 h and the FAM-positive cells were quantified by flow cytometry analysis. For the analysis of temperature-dependent cellular uptake, the cells were transfected with Ad4-3 LNP carrying FAM-labeled siRNA and incubated at 4°C or 37°C. The cells were re-suspended in 110 μL of PBS and applied to flow cytometry analysis.

Astrocyte-targeted siRNA delivery in mice model of TBI and in vivo RNAi efficiency

Balb/c mice (male, 8 weeks old) were purchased from Spife Biotechnology Company (Beijing, China). All animal experiments were approved by the animal care and use committee of Inner Mongolia University (approval number: 32160231). TBI model was performed as previously reported.[77] In brief, following anesthesia, an incision was made in the midline of the head. A core-shaped copper cooled with liquid nitrogen was placed stereotactically on the right parietal skull for 1 min (the area is 1.5 mm posterior, 1.5 mm lateral). Sham-operated mice went through the same procedure without placing the core-shaped copper. The mice were divided into four groups (three mice in each group): sham operation group; PBS-treated group: the TBI model was injected with PBS by i.v. injection; siCtrl and siTLR4 group: TBI model was injected with Ad4-3 LNP carrying either siCtrl or siTLR4 by i.v. injection. The dose of siRNA was 1 mg/kg body weight, and the corresponding dose of Ad4 LNP was 10 mg/kg body weight. After 24 h, the mice were killed for analysis of siRNA delivery efficiency. Total RNA and total protein were isolated from the lesion site of brain, and RT-qPCR and western blotting were performed for detecting the expression of TLR4 on mRNA and protein levels. For IHC analysis, the brain was sliced by vibratome (Leica VT 1200S, Switzerland), and was probed with primary antibodies for astrocyte marker (GFAP, Abcam, Cambridge, England), or microglia marker (Iba1, Abcam, Cambridge, England), or neuron marker (NeuN, Abcam, Cambridge, England), and visualized by secondary antibodies (goat anti-rabbit Alexa Fluor 594 conjugate, Abcam, Cambridge, England).

Western blot analysis

For *in vivo* experiments, the lesion site of brain was collected and lysed with TRIzol reagent, and the protein layer was extracted according to the protocol of TRIzol reagent. For *in vitro* experiments, C8-D1A cells treated with Ad4-3 LNP were washed three times with ice-cold PBS before being lysed with mammalian protein extraction reagent with protease inhibitor Cocktail (CWBioTech, Beijing, China). Protein concentration was determined using Pierce BCA protein assay (Thermo Fisher Scientific, MA, USA). All samples were heated in SDS-PAGE loading buffer at 95°C for 5 min before loading. After transferring the protein to polyvinylidene fluoride (PVDF) membrane and blocking, the primary antibodies (TLR4 Rabbit mAb, 1:1000, Bioss Antibodies, Beijing, China; GAPDH Rabbit mAb, 1:1000, Cell Signaling Technology, Danvers, MA, USA) were loaded and incubated with secondary antibody (Goat Anti-Rabbit IgG H&L [HRP], 1:4000, Abcam). Images were visualized by eECL Western blot kit (CW biotech, Beijing, China) and captured by Analytik jena UVP Chemstudio imaging system.

Organ distribution of siRNA delivered by Ad4-3 LNP in mice model of TBI

For the organ distribution study, sham group, FAM-labeled naked siTLR4, and Ad4-3 LNP carrying FAM-labeled siTLR4 were injected to TBI model mice, respectively. After 24 h, mice were intracardially perfused with normal saline and killed, and organs (liver, lung, heart, spleen, kidney, and brain) were harvested. *Ex vivo* fluorescence images of organs were obtained by UVP Ibox Scientia (Analytik Jena, Jena, Germany). The fluorescence intensity of brains was quantified by ImageJ.

Confocal microscope

The C8-D1A cells and brain slices were fixed in 4% paraformaldehyde, permeated in 0.1% Triton X-100. Then, the cells were stained with Phalloidin-iFluor 555 and DAPI. Brain slices were stained with corresponding primary antibodies and secondary antibodies sequentially. Images were obtained using a confocal microscope (Nikon AXR, Japan) at the channel of Ex/m = 556/574 nm; 460/550 nm; 358/461 nm.

The whole brain staining procedure was according to the manufacturer's protocol of Five-color mIHC kit (abs50029, absin, China). In brief, the fixed brain slices (5-μm thickness) were stained with first primary antibody and corresponding TSA secondary antibody sequentially. After the amplification of signals, slices were treated with antibody eluent, followed by staining with second, third antibodies and corresponding TSA secondary antibodies. After the mounting of slides, the whole slides were scanned by PANNORAMIC MIDI II (3D HISTECH, Hungary).

Determination of BBB integrity in mice by EB dye leakage

For evaluation of the BBB permeability or integrity, we used EB dye extravasation method, performed as per previous study.[59] After

injection of the dye, the skin color of mice changed immediately, and the brain lesions turned macroscopically blue. Four groups of mice (six mice in each group) were gently injected with 2% (w/v) EB dye (3 mL/kg) through the femoral vein. After 1 h, intracardial perfusion with normal saline was performed to remove the dye by circulation. After the brains were collected and weighed by analytical balance, the brain tissue was ground with 50% trichloroacetic acid, and the fluorescence intensity of the supernatant was measured at 620/680 nm using fluorescence intensity of EB dye in ethanol (100, 250, 500, 750, and 1000 ng/mL) as standard curve. The results were expressed as ng dye/mg brain tissue.

Measurement of serum cytokine level after knockdown of TLR4

To examine the consequences of Ad4-3 LNP-mediated knockdown of TLR4 in astrocytes in the TBI mouse model, we measured the expression of representative cytokines in serum. The expression level of representative anti-inflammatory cytokines (or A2 markers) and pro-inflammatory cytokines (or A1 markers) were quantified by ELISA kits (Thermo Fisher Scientific, MA, USA) according to the manufacturer's protocol.

Statistical analyses

All results were expressed as a mean ± standard deviation. Student's t test was used for statistical analysis between two groups and one-way ANOVA was used for multiple comparison test.

DATA AND CODE AVAILABILITY

Additional information on experimental procedures, materials, and methods including 1H NMR and 13C NMR spectra analysis for ionizable DoGo lipids, adenosine-conjugated DoGo lipids, figures for particle size distribution of LNPs, confocal images, and flow cytometry analysis of cellular uptake efficiency of LNPs, knockdown of adenosine receptors by ASO in C8-D1A cells, major organ distribution of Ad4-3 LNP carrying FAM-labeled siRNA, confocal image of brain slides, tables for formulations and characterization of LNPs, and tables for experimental primers and siRNA sequences are provided in supplemental information (PDF).

SUPPLEMENTAL INFORMATION

Supplemental information can be found online at https://doi.org/10.1016/j.omtn.2023.102065.

ACKNOWLEDGMENTS

Financial support was provided by National Natural Science Foundation of China (32160231) and Natural Science Foundation of Inner Mongolia Autonomous Region (2021MS02009).

AUTHOR CONTRIBUTIONS

H.X. and H.B. designed the study; H.S., C.C., and H.B. jointly supervised the study; H.X. performed experiments and analyzed the results; O.A., X.Y., Y.Z., X.H., and X.Y. assisted in chemical synthesis, *in vitro* studies, and animal experiments; H.X. and H.B. prepared the manuscript. All authors have reviewed and approved the submission.

DECLARATION OF INTERESTS

The authors declare no competing interests.

REFERENCES

1. Csobonyeiova, M., Polak, S., Zamborsky, R., and Danisovic, L. (2019). Recent Progress in the Regeneration of Spinal Cord Injuries by Induced Pluripotent Stem Cells. Int. J. Mol. Sci. *20*, 3838.
2. Li, W., Qiu, J., Li, X.L., Aday, S., Zhang, J., Conley, G., Xu, J., Joseph, J., Lan, H., Langer, R., et al. (2021). BBB pathophysiology-independent delivery of siRNA in traumatic brain injury. Sci. Adv. *7*, eabd6889.
3. Alam Bony, B., and Kievit, F.M. (2019). A Role for Nanoparticles in Treating Traumatic Brain Injury. Pharmaceutics *11*, 473.
4. Burda, J.E., Bernstein, A.M., and Sofroniew, M.V. (2016). Astrocyte roles in traumatic brain injury. Exp. Neurol. *275*, 305–315.
5. Pakkenberg, B., Pelvig, D., Marner, L., Bundgaard, M.J., Gundersen, H.J.G., Nyengaard, J.R., and Regeur, L. (2003). Aging and the human neocortex. Exp. Gerontol. *38*, 95–99.
6. Sun, Y., Ma, J., Li, D., Li, P., Zhou, X., Li, Y., He, Z., Qin, L., Liang, L., and Luo, X. (2019). Interleukin-10 inhibits interleukin-1beta production and inflammasome activation of microglia in epileptic seizures. J. Neuroinflammation *16*, 66.
7. Liddelow, S.A., and Barres, B.A. (2017). Reactive Astrocytes: Production, Function, and Therapeutic Potential. Immunity *46*, 957–967.
8. Liddelow, S.A., Guttenplan, K.A., Clarke, L.E., Bennett, F.C., Bohlen, C.J., Schirmer, L., Bennett, M.L., Münch, A.E., Chung, W.S., Peterson, T.C., et al. (2017). Neurotoxic reactive astrocytes are induced by activated microglia. Nature *541*, 481–487.
9. Barone, F.C., Arvin, B., White, R.F., Miller, A., Webb, C.L., Willette, R.N., Lysko, P.G., and Feuerstein, G.Z. (1997). Tumor necrosis factor-alpha. A mediator of focal ischemic brain injury. Stroke *28*, 1233–1244.
10. Rothwell, N., Allan, S., and Toulmond, S. (1997). The role of interleukin 1 in acute neurodegeneration and stroke: pathophysiological and therapeutic implications. J. Clin. Invest. *100*, 2648–2652.
11. Wang, J., Xing, H., Wan, L., Jiang, X., Wang, C., and Wu, Y. (2018). Treatment targets for M2 microglia polarization in ischemic stroke. Biomed. Pharmacother. *105*, 518–525.
12. Jiang, C.T., Wu, W.F., Deng, Y.H., and Ge, J.W. (2020). Modulators of microglia activation and polarization in ischemic stroke (Review). Mol. Med. Rep. *21*, 2006–2018.
13. Murray, P.J., Allen, J.E., Biswas, S.K., Fisher, E.A., Gilroy, D.W., Goerdt, S., Gordon, S., Hamilton, J.A., Ivashkiv, L.B., Lawrence, T., et al. (2014). Macrophage activation and polarization: nomenclature and experimental guidelines. Immunity *41*, 14–20.
14. Liu, X.L., Sun, D.D., Zheng, M.T., Li, X.T., Niu, H.H., Zhang, L., Zhou, Z.W., Rong, H.T., Wang, Y., Wang, J.W., et al. (2023). Maraviroc promotes recovery from traumatic brain injury in mice by suppression of neuroinflammation and activation of neurotoxic reactive astrocytes. Neural Regen. Res. *18*, 141–149.
15. Joy, M.T., Ben Assayag, E., Shabashov-Stone, D., Liraz-Zaltsman, S., Mazzitelli, J., Arenas, M., Abduljawad, N., Kliper, E., Korczyn, A.D., Thareja, N.S., et al. (2019). CCR5 Is a Therapeutic Target for Recovery after Stroke and Traumatic Brain Injury. Cell *176*, 1143–1157.e13.
16. Khadka, B., Lee, J.Y., Kim, K.T., and Bae, J.S. (2020). Recent progress in therapeutic drug delivery systems for treatment of traumatic CNS injuries. Future Med. Chem. *12*, 1759–1778.
17. Su, L., Athamna, M., Wang, Y., Wang, J., Freudenberg, M., Yue, T., Wang, J., Moresco, E.M.Y., He, H., Zor, T., et al. (2021). Sulfatides Are Endogenous Ligands for the TLR4-MD-2 Complex. Proc. Natl. Acad. Sci. USA *118*.
18. Xiao, H., Altangerel, A., Gerile, G., Wu, Y., and Baigude, H. (2016). Design of Highly Potent Lipid-Functionalized Peptidomimetics for Efficient in Vivo siRNA Delivery. ACS Appl. Mater. Interfaces *8*, 7638–7645.
19. Xiao, H., Han, S., and Baigude, H. (2021). Regulation of microglia polarization via mannose receptor-mediated delivery of siRNA by ligand-functionalized DoGo LNP. RSC Adv. *11*, 32549–32558.
20. Paunovska, K., Loughrey, D., and Dahlman, J.E. (2022). Drug delivery systems for RNA therapeutics. Nat. Rev. Genet. *23*, 265–280.

21. Yonezawa, S., Koide, H., and Asai, T. (2020). Recent advances in siRNA delivery mediated by lipid-based nanoparticles. Adv. Drug Deliv. Rev. *154–155*, 64–78.

22. Thomas, M., Kularatne, S.A., Qi, L., Kleindl, P., Leamon, C.P., Hansen, M.J., and Low, P.S. (2009). Ligand-targeted delivery of small interfering RNAs to malignant cells and tissues. Ann. N. Y. Acad. Sci. *1175*, 32–39.

23. Wittrup, A., and Lieberman, J. (2015). Knocking down disease: a progress report on siRNA therapeutics. Nat. Rev. Genet. *16*, 543–552.

24. Whitehead, K.A., Langer, R., and Anderson, D.G. (2009). Knocking down barriers: advances in siRNA delivery. Nat. Rev. Drug Discov. *8*, 129–138.

25. Sakurai, Y., Mizumura, W., Ito, K., Iwasaki, K., Katoh, T., Goto, Y., Suga, H., and Harashima, H. (2020). Improved Stability of siRNA-Loaded Lipid Nanoparticles Prepared with a PEG-Monoacyl Fatty Acid Facilitates Ligand-Mediated siRNA Delivery. Mol. Pharm. *17*, 1397–1404.

26. Thi, T.T.H., Suys, E.J.A., Lee, J.S., Nguyen, D.H., Park, K.D., and Truong, N.P. (2021). Lipid-Based Nanoparticles in the Clinic and Clinical Trials: From Cancer Nanomedicine to COVID-19 Vaccines. Vaccines (Basel) *9*.

27. Hou, X., Zaks, T., Langer, R., and Dong, Y. (2021). Lipid nanoparticles for mRNA delivery. Nat. Rev. Mater. *6*, 1078–1094.

28. Chang, R.Y.K., and Chan, H.K. (2021). Lipid nanoparticles for the inhalation of mRNA. Nat. Biomed. Eng. *5*, 949–950.

29. Witzigmann, D., Kulkarni, J.A., Leung, J., Chen, S., Cullis, P.R., and van der Meel, R. (2020). Lipid nanoparticle technology for therapeutic gene regulation in the liver. Adv. Drug Deliv. Rev. *159*, 344–363.

30. Maugeri, M., Nawaz, M., Papadimitriou, A., Angerfors, A., Camponeschi, A., Na, M., Hölttä, M., Skantze, P., Johansson, S., Sundqvist, M., et al. (2019). Linkage between endosomal escape of LNP-mRNA and loading into EVs for transport to other cells. Nat. Commun. *10*, 4333.

31. Zhao, Z., Ukidve, A., Kim, J., and Mitragotri, S. (2020). Targeting Strategies for Tissue-Specific Drug Delivery. Cell *181*, 151–167.

32. Miyazaki, T., Nakagawa, Y., and Cabral, H. (2021). Chapter 24-Strategies for ligand-installed nanocarriers. In Handbook of Nanotechnology Applications, W.J. Lau, K. Faungnawakij, K. Piyachomkwan, and U.R. Ruktanonchai, eds. (Elsevier), pp. 633–655.

33. Srinivasarao, M., and Low, P.S. (2017). Ligand-Targeted Drug Delivery. Chem. Rev. *117*, 12133–12164.

34. Kapoor, D., Bhatt, S., Kumar, M., Maheshwari, R., and Tekade, R.K. (2019). Chapter 8 - Ligands for Targeted Drug Delivery and Applications. In Basic Fundamentals of Drug Delivery, R.K. Tekade, ed. (Academic Press), pp. 307–342.

35. Molina, M.A., Codony-Servat, J., Albanell, J., Rojo, F., Arribas, J., and Baselga, J. (2001). Trastuzumab (herceptin), a humanized anti-Her2 receptor monoclonal antibody, inhibits basal and activated Her2 ectodomain cleavage in breast cancer cells. Cancer Res. *61*, 4744–4749.

36. Wong, S.F. (2005). Cetuximab: an epidermal growth factor receptor monoclonal antibody for the treatment of colorectal cancer. Clin. Therapeut. *27*, 684–694.

37. Daniels, T.R., Bernabeu, E., Rodríguez, J.A., Patel, S., Kozman, M., Chiappetta, D.A., Holler, E., Ljubimova, J.Y., Helguera, G., and Penichet, M.L. (2012). The transferrin receptor and the targeted delivery of therapeutic agents against cancer. Biochim. Biophys. Acta *1820*, 291–317.

38. Sobot, D., Mura, S., Rouquette, M., Vukosavljevic, B., Cayre, F., Buchy, E., Pieters, G., Garcia-Argote, S., Windbergs, M., Desmaële, D., and Couvreur, P. (2017). Circulating Lipoproteins: A Trojan Horse Guiding Squalenoylated Drugs to LDL-Accumulating Cancer Cells. Mol. Ther. *25*, 1596–1605.

39. Sobot, D., Mura, S., Yesylevskyy, S.O., Dalbin, L., Cayre, F., Bort, G., Mougin, J., Desmaële, D., Lepetre-Mouelhi, S., Pieters, G., et al. (2017). Conjugation of squalene to gemcitabine as unique approach exploiting endogenous lipoproteins for drug delivery. Nat. Commun. *8*, 15678.

40. Farokhzad, O.C., Jon, S., Khademhosseini, A., Tran, T.N.T., Lavan, D.A., and Langer, R. (2004). Nanoparticle-aptamer bioconjugates: a new approach for targeting prostate cancer cells. Cancer Res. *64*, 7668–7672.

41. Fernández, M., Javaid, F., and Chudasama, V. (2018). Advances in targeting the folate receptor in the treatment/imaging of cancers. Chem. Sci. *9*, 790–810.

42. Uchida, Y., Ohtsuki, S., Katsukura, Y., Ikeda, C., Suzuki, T., Kamiie, J., and Terasaki, T. (2011). Quantitative targeted absolute proteomics of human blood-brain barrier transporters and receptors. J. Neurochem. *117*, 333–345.

43. Anraku, Y., Kuwahara, H., Fukusato, Y., Mizoguchi, A., Ishii, T., Nitta, K., Matsumoto, Y., Toh, K., Miyata, K., Uchida, S., et al. (2017). Glycaemic control boosts glucosylated nanocarrier crossing the BBB into the brain. Nat. Commun. *8*, 1001.

44. Low, P.S., Henne, W.A., and Doorneweerd, D.D. (2008). Discovery and development of folic-acid-based receptor targeting for imaging and therapy of cancer and inflammatory diseases. Acc. Chem. Res. *41*, 120–129.

45. Fredholm, B.B., Abbracchio, M.P., Burnstock, G., Dubyak, G.R., Harden, T.K., Jacobson, K.A., Schwabe, U., and Williams, M. (1997). Towards a revised nomenclature for P1 and P2 receptors. Trends Pharmacol. Sci. *18*, 79–82.

46. Ribeiro, J.A., Sebastião, A.M., and de Mendonça, A. (2002). Adenosine receptors in the nervous system: pathophysiological implications. Prog. Neurobiol. *68*, 377–392.

47. Ganbold, T., Bao, Q., Xiao, H., Zurgaanjin, D., Liu, C., Han, S., Hasi, A., and Baigude, H. (2022). Peptidomimetic Lipid-Nanoparticle-Mediated Knockdown of TLR4 in CNS Protects against Cerebral Ischemia/Reperfusion Injury in Mice. Nanomaterials *12*, 2072.

48. Ganbold, T., Bao, Q., Zandan, J., Hasi, A., and Baigude, H. (2020). Modulation of Microglia Polarization through Silencing of NF-kappaB p65 by Functionalized Curdlan Nanoparticle-Mediated RNAi. ACS Appl. Mater. Interfaces *12*, 11363–11374.

49. Liu, G., Zhang, W., Guo, J., Kong, F., Zhou, S., Chen, S., Wang, Z., and Zang, D. (2018). Adenosine binds predominantly to adenosine receptor A1 subtype in astrocytes and mediates an immunosuppressive effect. Brain Res. *1700*, 47–55.

50. Haskó, G., Pacher, P., Vizi, E.S., and Illes, P. (2005). Adenosine receptor signaling in the brain immune system. Trends Pharmacol. Sci. *26*, 511–516.

51. Bao, Q., Ganbold, T., Qiburi, Q., Bao, M., Han, S., and Baigude, H. (2021). AMP functionalized curdlan nanoparticles as a siRNA carrier: Synthesis, characterization and targeted delivery via adenosine A(2B) receptor. Int. J. Biol. Macromol. *193*, 866–873.

52. Han, X., Zhang, H., Butowska, K., Swingle, K.L., Alameh, M.G., Weissman, D., and Mitchell, M.J. (2021). An ionizable lipid toolbox for RNA delivery. Nat. Commun. *12*, 7233.

53. Semple, S.C., Akinc, A., Chen, J., Sandhu, A.P., Mui, B.L., Cho, C.K., Sah, D.W.Y., Stebbing, D., Crosley, E.J., Yaworski, E., et al. (2010). Rational design of cationic lipids for siRNA delivery. Nat. Biotechnol. *28*, 172–176.

54. Jayaraman, M., Ansell, S.M., Mui, B.L., Tam, Y.K., Chen, J., Du, X., Butler, D., Eltepu, L., Matsuda, S., Narayanannair, J.K., et al. (2012). Maximizing the potency of siRNA lipid nanoparticles for hepatic gene silencing *in vivo*. Angew. Chem. Int. Ed. Engl. *51*, 8529–8533.

55. Patel, P., Ibrahim, N.M., and Cheng, K. (2021). The Importance of Apparent pKa in the Development of Nanoparticles Encapsulating siRNA and mRNA. Trends Pharmacol. Sci. *42*, 448–460.

56. Fang, J., Nakamura, H., and Maeda, H. (2011). The EPR effect: Unique features of tumor blood vessels for drug delivery, factors involved, and limitations and augmentation of the effect. Adv. Drug Deliv. Rev. *63*, 136–151.

57. Chen, S., Tam, Y.Y.C., Lin, P.J.C., Leung, A.K.K., Tam, Y.K., and Cullis, P.R. (2014). Development of lipid nanoparticle formulations of siRNA for hepatocyte gene silencing following subcutaneous administration. J. Contr. Release *196*, 106–112.

58. Zahir-Jouzdani, F., Mottaghitalab, F., Dinarvand, M., and Atyabi, F. (2018). siRNA delivery for treatment of degenerative diseases, new hopes and challenges. J. Drug Deliv. Sci. Technol. *45*, 428–441.

59. Goldim, M.P.d.S., Della Giustina, A., and Petronilho, F. (2019). Using Evans Blue Dye to Determine Blood-Brain Barrier Integrity in Rodents. Curr. Protoc. Im. *126*, e83.

60. Kimura, S., and Harashima, H. (2020). Current Status and Challenges Associated with CNS-Targeted Gene Delivery across the BBB. Pharmaceutics *12*, 1216.

61. Saunus, J.M., McCart Reed, A.E., Lim, Z.L., and Lakhani, S.R. (2017). Breast Cancer Brain Metastases: Clonal Evolution in Clinical Context. Int. J. Mol. Sci. *18*, 152.

62. Wu, D., Chen, Q., Chen, X., Han, F., Chen, Z., and Wang, Y. (2023). The blood-brain barrier: structure, regulation, and drug delivery. Signal Transduct. Targeted Ther. *8*, 217.

63. Thoren, A.E., Helps, S.C., Nilsson, M., and Sims, N.R. (2005). Astrocytic function assessed from 1-14C-acetate metabolism after temporary focal cerebral ischemia in rats. J. Cerebr. Blood Flow Metabol. *25*, 440–450.

64. Anderson, M.F., Blomstrand, F., Blomstrand, C., Eriksson, P.S., and Nilsson, M. (2003). Astrocytes and stroke: networking for survival? Neurochem. Res. *28*, 293–305.

65. Almeida, A., Jimenez-Blasco, D., and Bolaños, J.P. (2023). Cross-talk between energy and redox metabolism in astrocyte-neuron functional cooperation. Essays Biochem. *67*, 17–26.

66. Kumar, A., and Loane, D.J. (2012). Neuroinflammation after traumatic brain injury: opportunities for therapeutic intervention. Brain Behav. Immun. *26*, 1191–1201.

67. Michinaga, S., and Koyama, Y. (2021). Pathophysiological Responses and Roles of Astrocytes in Traumatic Brain Injury. Int. J. Mol. Sci. *22*, 6418.

68. Zhou, Y., Zhu, F., Liu, Y., Zheng, M., Wang, Y., Zhang, D., Anraku, Y., Zou, Y., Li, J., Wu, H., et al. (2020). Blood-brain barrier-penetrating siRNA nanomedicine for Alzheimer's disease therapy. Sci. Adv. *6*, eabc7031.

69. Verkhratsky, A., Parpura, V., Vardjan, N., and Zorec, R. (2019). Physiology of Astroglia. Adv. Exp. Med. Biol. *1175*, 45–91.

70. Bao, Q., Ganbold, T., Bao, M., Xiao, H., Han, S., and Baigude, H. (2023). Tumor targeted siRNA delivery by adenosine receptor-specific curdlan nanoparticles. Int. J. Biol. Macromol. *253*, 126845.

71. Yuan, M., and Wu, H. (2022). Astrocytes in the Traumatic Brain Injury: the Good and the Bad. Exp. Neurol. *348*, 113943.

72. Sharma, V.K., Osborn, M.F., Hassler, M.R., Echeverria, D., Ly, S., Ulashchik, E.A., Martynenko-Makaev, Y.V., Shmanai, V.V., Zatsepin, T.S., Khvorova, A., and Watts, J.K. (2018). Novel Cluster and Monomer-Based GalNAc Structures Induce Effective Uptake of siRNAs in Vitro and in Vivo. Bioconjugate Chem. *29*, 2478–2488.

73. Jiang, H., Wang, Y., Liang, X., Xing, X., Xu, X., and Zhou, C. (2018). Toll-Like Receptor 4 Knockdown Attenuates Brain Damage and Neuroinflammation After Traumatic Brain Injury via Inhibiting Neuronal Autophagy and Astrocyte Activation. Cell. Mol. Neurobiol. *38*, 1009–1019.

74. Azam, S., Jakaria, M., Kim, I.S., Kim, J., Haque, M.E., and Choi, D.K. (2019). Regulation of Toll-Like Receptor (TLR) Signaling Pathway by Polyphenols in the Treatment of Age-Linked Neurodegenerative Diseases: Focus on TLR4 Signaling. Front. Immunol. *10*, 1000.

75. Leib, D., Chen, Y.H., Monteys, A.M., and Davidson, B.L. (2022). Limited astrocyte-to-neuron conversion in the mouse brain using NeuroD1 overexpression. Mol. Ther. *30*, 982–986.

76. Milner, R., Hung, S., Wang, X., Berg, G.I., Spatz, M., and del Zoppo, G.J. (2008). Responses of endothelial cell and astrocyte matrix-integrin receptors to ischemia mimic those observed in the neurovascular unit. Stroke *39*, 191–197.

77. Raslan, F., Albert-Weißenberger, C., Ernestus, R.I., Kleinschnitz, C., and Sirén, A.L. (2012). Focal brain trauma in the cryogenic lesion model in mice. Exp. Transl. Stroke Med. *4*, 6.